The Aeronautical Journal (2024), **128**, pp. 1627–1651
doi:10.1017/aer.2024.2

ROYAL AERONAUTICAL SOCIETY

RESEARCH ARTICLE

Fixed-time anti-saturation control with concise system structure for the 6-DOF motion of spacecraft

X. Wei[1], Y. Tian[1], S. Wu[1], D. Zhang[1], X. Shao[1] and L. Chen[2]

[1]School of Aeronautics and Astronautics, Shanghai Jiao Tong University, Shanghai, China and [2]Beijing Institute of Tracking and Telecommunication Technology, Beijing, China
Corresponding author: X. Shao; Email: shaoxwmail@163.com

Received: 14 July 2023; **Revised:** 14 November 2023; **Accepted:** 3 January 2024

Keywords: Fixed time; anti-saturation; spacecraft; disturbance observer; sliding mode control

Abstract

This paper proposes a fixed-time anti-saturation (FT-AS) control scheme with a simple control loop for the 6-Degree-of-Freedom tracking (6-DOF) control problem of spacecraft with parameter uncertainties, external disturbances and input saturation. Considering the external disturbance and parameter uncertainties, the dynamical model of the tracking error is established. The traditional methods of handling input saturation usually add anti-saturation subsystems in the control system to suppress the impact of input overshoot. However, this paper directly inputs the input overshoot into the tracking error model, thus constructing a modified lumped disturbance term that includes the influence of input overshoot. Then, a novel fixed-time disturbance observer (FT-DO) is designed to estimate and compensate for this modified lumped disturbance. Therefore, there is no need to add the anti-saturation structures in the control loop, significantly reducing the complexity of the system. Finally, an observer-based fixed-time non-singular terminal sliding mode (FT-NTSM) controller is designed to guarantee the fixed-time stability of the whole system. In this way, the convergence time of the proposed scheme does not depend on the system's initial conditions. Simulation results illustrate that the proposed method keeps the control input within the limit while achieving high-precision tracking control of attitude and position.

Nomenclature

a	semi-major axis, km
$B-x_0y_0z_0$	Radial-Transverse-Normal (RTN) coordinate system
$\boldsymbol{d}$	$=[\boldsymbol{d}_b{}^T, \boldsymbol{d}_a{}^T]^T$, lumped disturbance
$\hat{\boldsymbol{d}}$	estimated value of lumped disturbance
$\boldsymbol{d}_s$	modified lumped disturbance including input overshoot
$\hat{\boldsymbol{d}}_s$	estimated value of d_s
$\boldsymbol{d}_f$	disturbance force, N
$\boldsymbol{d}_\tau$	disturbance torque, Nm
$\boldsymbol{e}$	$=[\boldsymbol{e}_1{}^T, \boldsymbol{e}_2{}^T]^T$, state vector of tracking error dynamical system
$\boldsymbol{e}_o$	$=[\boldsymbol{e}_{o1}{}^T, \boldsymbol{e}_{o2}{}^T]^T$, estimation error
$\bar{e}$	eccentricity
$\boldsymbol{f}$	control force, N
i	inclination, deg
$\boldsymbol{J}$	spacecraft's moment of inertia, kgm^2
$\boldsymbol{J}_o$	nominal moment of inertia, kgm^2
M_o	mean anomaly, deg
m	mass of spacecraft, kg
m_o	nominal mass, kg
p	parameter of observer

$O-XYZ$	Earth Centered Inertial (ECI) coordinate system
p_k	($k=1,2$), parameter of controller. q_k, m_k, n_k, (k= 1, 2) are also controller parameters
$\boldsymbol{r}$	position vector in ECI frame, m
$\boldsymbol{s}$	sliding mode surface
S_b	spacecraft body-fixed frame
T_c	bound of convergence time of states of spacecraft error system
T_o	bound of convergence time of observer
T_s	sum of the time of the error system state reaching the sliding surface and T_o
T_ε	transit time from P_2 to P_1
$\boldsymbol{u}$	control input
$\boldsymbol{u_T}$	control input of traditional method
$\boldsymbol{u_i}$	actual controller output without saturation limit
$\boldsymbol{v}$	velocity vector in ECI frame, m/s
$\boldsymbol{w}$	angular velocity, rad/s

Subscripts

t	desired value
e	error

Greek Symbol

γ	switching gain
$\boldsymbol{\Delta} J$	uncertainty of moment of inertia, kgm^2
Δm	uncertainty of mass, kg
$\boldsymbol{\Delta} u$	the auxiliary variable
$\boldsymbol{\vartheta}$	$=[\boldsymbol{\vartheta_1}^T \boldsymbol{\vartheta_2}^T]^T$, state vector of observer
λ_k	($k=1,2,3.$) parameters of observer
ν_k	($k=1,2$), parameter of controller; η_k ($k=1,2$) is also controller parameter
μ_g	gravitational constant of the Earth, m^{3}s^{-2}
$\boldsymbol{\sigma}$	MRP attitude
$\boldsymbol{\tau}$	control torque, Nm
Ω	right ascension of ascending node, deg
ω	argument of perigee, deg

1.0 Introduction

In many scenarios, such as rendezvous and docking and satellite formation flying, high-precision integrated attitude and orbit tracking control, also known as 6-Degree-of-Freedom (6-DOF) tracking control, guarantees the implementation of space missions. Hence, there has been a growing interest in 6-DOF tracking control [1–5]. However, the strong non-linearity, parameter uncertainties, complex disturbances from the spatial environment, and limited actuator capabilities have posed significant challenges for the design of spacecraft controllers [6–8]. In this paper, a more concise control loop will be designed under these adverse conditions to achieve fixed-time convergence of the 6-DOF tracking errors for spacecraft.

In the past few decades, sliding mode control has been widely applied to stabilise nonlinear systems due to its excellent robustness against disturbances and parameter uncertainties [9–13]. In sliding mode control, researchers have continued to explore the optimisation of system convergence time. The optimisation of convergence time has driven the evolution of sliding mode control from asymptotic stability to finite-time stability and further to fixed-time stability. For instance, sliding mode controllers for asymptotic and finite-time stability are designed to achieve tracking control of spacecraft in the presence of

https://doi.org/10.1017/aer.2024.2 Published online by Cambridge University Press

external disturbances and parameter uncertainties [14–17]. However, for asymptotic stability, the convergence time is too long, and, for finite-time stability, the upper bound of the convergence time depends on the system's initial state, which is difficult to determine for systems with parameter uncertainties [18]. Therefore, the research on control schemes that converge without relying on the initial state is of practical significance. In 2012, Polyakov et al. proposed the concept of fixed-time stability, which means that the convergence time of the system has an upper bound independent of the system's initial state [18, 19]. The control scheme optimises the system convergence time and has more practical significance [20]. In recent years, there has been extensive research on fixed-time control in the aerospace field. For the attitude control of spacecraft, the fixed-time sliding mode controllers were designed to reduce the convergence time of the attitude error [21, 22]. For 6-DOF control of spacecraft, the fixed-time sliding mode controllers were designed [23, 24], which have faster convergence performance than fast terminal sliding mode. Inspired by the mentioned literature, this paper will further investigate the application of fixed-time sliding mode control in the spacecraft's 6-DOF tracking control.

In addition, parameter uncertainty and external disturbances can also significantly impact the convergence accuracy and speed of control systems [25, 26]. A commonly used approach to mitigate these adverse effects is the implementation of disturbance observers [27, 28]. The finite-time disturbance observer and controller have been designed for spacecraft subjected to external disturbances, enabling the spacecraft's states to converge to equilibrium within a finite time [29]. Since the convergence time of the observer directly affects the overall system convergence time, if the convergence time of the error observation subsystem is also designable and independent of the initial state, it will contribute to controlling the convergence time of the entire system. For example, Wu et al. designed fixed-time disturbance observers and controllers, achieving fixed-time convergence of the spacecraft system. However, this fixed-time control scheme did not consider the impact of input saturation [24]. Actually, there is a relatively limited amount of research on fixed-time control for spacecraft that simultaneously considers parameter uncertainty, external disturbances and input saturation.

However, the adverse effect of input saturation will reduce the control accuracy and even lead to system instability [30]. To eliminate the adverse impact of input overshoot between the expected and the actual control inputs, the auxiliary systems are designed to compensate for it [30–32]. An anti-windup saturation compensator was designed to avoid the adverse effects of actuator saturation for the orbit control of satellite formation flying [33]. For the proximity operations of the spacecraft, a linear compensator system was designed to deal with control input saturation [28]. Assume the auxiliary variable Δu represents the overshoot between the actual output of the controller u_i and the saturation limit. The above methods introduce an additional anti-saturation structure in the system, as shown in Fig. 1, which increases the complexity of system dynamics and brings difficulties to the design of the control system.

To simplify the control loop illustrated in Fig. 1, this paper proposes a fixed-time anti-saturation control (FT-AS) scheme with a more concise structure for the spacecraft's 6-DOF tracking control, as shown in Fig. 2. The proposed FT-AS method can effectively handle parameter uncertainties, external disturbances and input saturation while achieving fixed-time convergence of the entire system. The main contributions of this paper are as follows:

- A new approach for handling input saturation has been proposed. In the traditional method, the input overshoot Δu is suppressed through an anti-saturation subsystem (as shown in Fig. 1). However, in this paper, the overshoot Δu is input into the tracking error model (as shown in Fig. 2), and its impact is transformed into a specific disturbance term. This disturbance term is then combined with parameter uncertainties and external disturbances to form a modified lumped disturbance d_s. A fixed-time disturbance observer (FT-DO) is designed to observe the modified lumped disturbances.
- The control loop has been simplified. The proposed FT-DO has the capability to handle input saturation. There is no need to introduce additional anti-saturation structures in the control loop, thereby greatly simplifying the control system structure.

https://doi.org/10.1017/aer.2024.2 Published online by Cambridge University Press

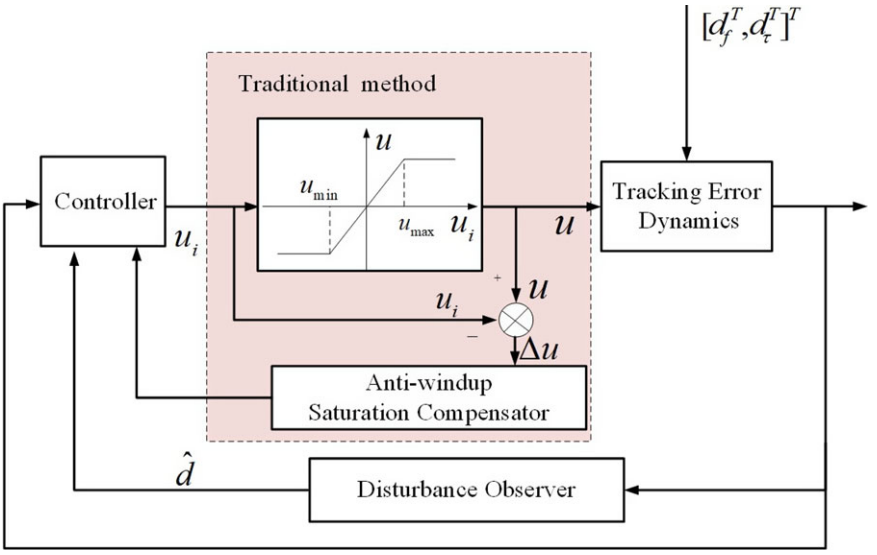

Figure 1. *Traditional anti-saturation control block diagram.*

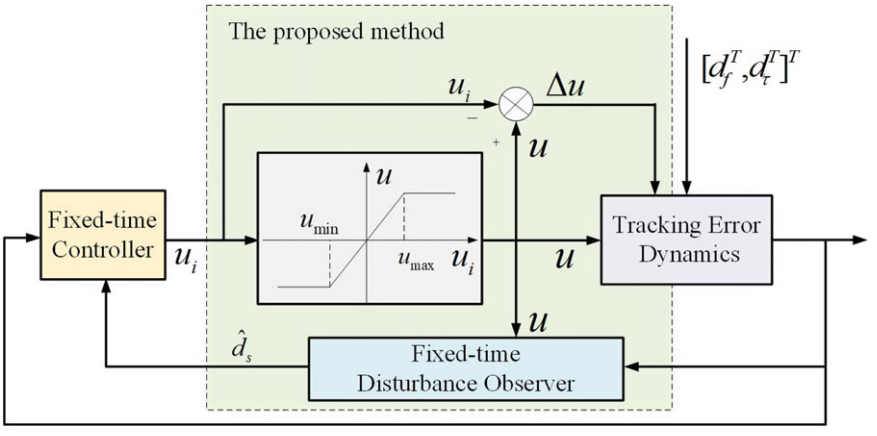

Figure 2. *Control block diagram of the proposed FT-AS control method.*

- The entire control system is fixed-time stable, and the convergence time of the tracking error is independent of the system's initial state. The FT-DO ensures the fixed-time stability of the estimation error dynamic subsystem, and a fixed-time nonsingular terminal sliding mode (FT-NTSM) controller is designed to guarantee the fixed-time stability of the tracking error system. Compared to traditional approaches, this scheme can achieve comparable or higher control accuracy while ensuring that the inputs meet the constraints.

This paper is organised as follows. In Section 2, the control objective is introduced, and the tracking error model is established. In Section 3, the FT-DO is designed for the modified lumped disturbance. In Section 4, the FT-NTSM controller is designed, and the stability of the whole system is proved. Numerical simulations are presented in Section 5 to demonstrate the effectiveness of the proposed control method. Section 6 gives the conclusion.

https://doi.org/10.1017/aer.2024.2 Published online by Cambridge University Press

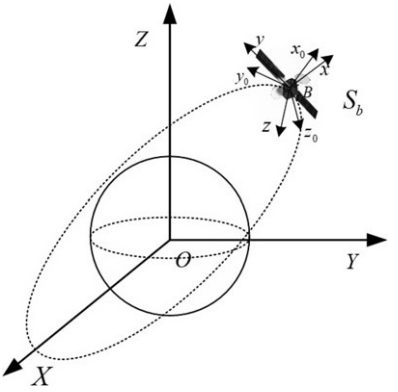

Figure 3. *Coordinate system (ECI coordinate system $O-XYZ$, RTN coordinate system $B-x_0y_0z_0$, spacecraft body-fixed coordinate system $B-xyz$).*

2.0 Problem statement

2.1 Control objective

The control block diagram of the proposed 6-DOF fixed-time anti-saturation control scheme is illustrated in Fig. 2. It is necessary to establish an error model between the actual and the desired trajectories to achieve tracking of the desired trajectory. The desired position and attitude can be expressed as $\boldsymbol{r}_t \in \mathbb{R}^3$ and $\boldsymbol{\sigma}_t \in \mathbb{R}^3$. The actual states of the spacecraft are $\boldsymbol{r}$ and $\boldsymbol{\sigma}$, and the tracking error states are expressed by $\boldsymbol{e}_l = [(\boldsymbol{r}_e)^T, (\boldsymbol{\sigma}_e)^T]^T$, where $\boldsymbol{r}_e$ and $\boldsymbol{\sigma}_e$ are the position error and the attitude error, respectively. The control objective is to converge tracking errors to zero ($\boldsymbol{e}_l \to \boldsymbol{0}$) in a fixed time. As illustrated in Fig. 2, $\boldsymbol{u}_i$ is the actual controller output, and $\hat{\boldsymbol{d}}_s$ is the estimate of the modified lumped disturbance, which includes the influence caused by input overshoot.

2.2 Definitions and notations

The coordinate systems of orbital and attitude motion are shown in Fig. 3. $\{O-XYZ\}$ is the Earth Centered Inertial (ECI) coordinate system. The origin O is located at the centre of the Earth. The $O-XY$ plane coincides with the equatorial plane of the Earth. The X-axis points to the vernal equinox, the Z-axis points to the North Pole, and the Y-axis, X-axis and Z-axis form a right-handed coordinate system. $\{B-x_0y_0z_0\}$ is the RTN (Radial-Transverse-Normal) coordinate system, which is used as the reference coordinate system of attitude. The origin B is located at the centre of mass of the spacecraft. The direction of $B-x_0$ points from the Earth towards the spacecraft, while the $B-y_0$ direction lies within the orbital plane, perpendicular to the $B-x_0$ axis, and points towards the direction of spacecraft motion. The $B-z_0$ axis forms a right-handed coordinate system with the $B-x_0$ and $B-y_0$ axes. $S_b\Delta = \{B-xyz\}$ is the spacecraft body-fixed frame, whose axes are aligned with the orthogonal inertial principal axes to form a right-handed coordinate system.

Definition 1. For a vector $\boldsymbol{\chi} = [\chi_1 \quad \chi_2 \quad \chi_3]^T$, $\psi(\boldsymbol{\chi}) \in \mathbb{R}^{3\times3}$ is defined as

$$\psi(\boldsymbol{\chi}) = \begin{bmatrix} 0 & -\chi_3 & \chi_2 \\ \chi_3 & 0 & -\chi_1 \\ -\chi_2 & \chi_1 & 0 \end{bmatrix} \tag{1}$$

Then, the cross product of $\boldsymbol{\chi}$ and any vector $\boldsymbol{\Upsilon} \in \mathbb{R}^3$ can be expressed as $\psi(\chi)\,\boldsymbol{\Upsilon}$.

Definition 2. [34] Consider a control system $\dot{\boldsymbol{\chi}}(\boldsymbol{t}) = \boldsymbol{u}(t) + \boldsymbol{\zeta}(t)$ with $\boldsymbol{\chi}(t_0) = \boldsymbol{\chi_0}$, where $\boldsymbol{\chi}(t)$ is the state variable, $\boldsymbol{u}(\boldsymbol{t})$ is the control input, and $\boldsymbol{\zeta}(\boldsymbol{t})$ is the bounded disturbance satisfying the Lipschitz condition.

https://doi.org/10.1017/aer.2024.2 Published online by Cambridge University Press

If the system is fixed-time convergent to the origin, there exists a time moment T (independent of the initial state $\boldsymbol{\chi_0}$) such that for all $t > T$, the state variable equals zero $\boldsymbol{\chi}(t) = 0$, regardless of the initial condition $\boldsymbol{\chi}_0$.

Notation 1. *$\|\cdot\|$ is the 2-norm of a vector or matrix. $diag(\cdot)$ represents the diagonal matrix. O_n and I_n represent the zero matrix and the identity matrix of $n \times n$, respectively.*

Notation 2. *For a vector $\boldsymbol{\chi} = [\chi_1 \quad \chi_2 \quad \dots \quad \chi_n]^T$, $sig^z(\boldsymbol{\chi}) = [|\chi_1|^z sign(\chi_1), |\chi_2|^z sign(\chi_2), \dots, |\chi_n|^z sign(\chi_n)]^T$, where $sign(\cdot)$ is the Signum function.*

Notation 3. *The vectors $\boldsymbol{X_1} = [1, \underbrace{0, 0 \dots 0}_{n-1}], \boldsymbol{X_2} = [0, 1, \underbrace{0 \dots 0}_{n-2}], \dots, \boldsymbol{X_n} = [\underbrace{0, 0 \dots 0}_{n-1}, 1]$ and matrices*

$$\boldsymbol{E_1} = \begin{bmatrix} 1 & 0 & \cdots & 0 \\ 0 & 0 & \cdots & 0 \\ & & & \\ 0 & 0 & \ddots & \vdots \\ 0 & 0 & \cdots & 0 \end{bmatrix}_{n\times n}, \boldsymbol{E_2} = \begin{bmatrix} 0 & 0 & \cdots & 0 \\ 0 & 1 & \cdots & 0 \\ & & & \\ 0 & 0 & \ddots & \vdots \\ 0 & 0 & \cdots & 0 \end{bmatrix}_{n\times n}, \dots, \boldsymbol{E_n} = \begin{bmatrix} 0 & 0 & \cdots & 0 \\ 0 & 0 & \cdots & 0 \\ & & & \\ 0 & 0 & \ddots & \vdots \\ 0 & 0 & \cdots & 1 \end{bmatrix}_{n\times n}$$

are defined. For a vector $\boldsymbol{\chi} = [\chi_1 \quad \chi_2 \quad \dots \quad \chi_n]$, the diagonal matrix formed by the elements of vector $\boldsymbol{\chi}$ can be expressed as $diag(\boldsymbol{\chi}) = \sum_{m=1}^{n} (\boldsymbol{\chi} * \boldsymbol{X_m^T} * \boldsymbol{E_m}) = \begin{bmatrix} \chi_1 & 0 & 0 \\ 0 & \ddots & 0 \\ 0 & 0 & \chi_n \end{bmatrix}$.

2.3 Spacecraft model

2.3.1 Spacecraft dynamics with external disturbance and parameter uncertainties

In this paper, the orbital dynamic equations are expressed in the ECI coordinate system, and the attitude kinematic and dynamic equations are expressed in the S_b coordinate system. To streamline the control law derivation and mitigate singularity issues in attitude kinematics, Modified Rodrigues Parameters (MRPs) are used to represent the attitude. Consequently, the satellite dynamics is formulated as [35]

$$\begin{cases} \dot{\boldsymbol{r}} = \boldsymbol{v} \\ m\dot{\boldsymbol{v}} + m\mu\boldsymbol{r} = \boldsymbol{f} + \boldsymbol{d}_f \\ \dot{\boldsymbol{\sigma}} = G(\boldsymbol{\sigma})\boldsymbol{w} \\ \boldsymbol{J}\dot{\boldsymbol{w}} + \psi(\boldsymbol{w})\boldsymbol{J}\boldsymbol{w} = \tau + \boldsymbol{d}_\tau \end{cases} \tag{2}$$

where $G(\boldsymbol{\sigma})$ is defined as $G(\boldsymbol{\sigma}) = \left[\left(1 - \boldsymbol{\sigma}^T\boldsymbol{\sigma}\right) I_3 + 2\psi(\boldsymbol{\sigma}) + 2\boldsymbol{\sigma}\boldsymbol{\sigma}^T\right]/4$, and it is nonsingular. $\boldsymbol{r} \in \mathbb{R}^3$ and $\boldsymbol{v} \in \mathbb{R}^3$ are the position and velocity vectors, respectively. m is the mass of the spacecraft. $\mu = \mu_g/\|\boldsymbol{r}\|^3$, where μ_g is the geocentric gravitational constant. $\boldsymbol{\sigma} = [\sigma_1, \sigma_2, \sigma_3]^T$ is the MRPs. $\boldsymbol{w} \in \mathbb{R}^3$ is the angular velocity. $\boldsymbol{f}$ and $\boldsymbol{\tau}$ are the control force and torque. $\boldsymbol{d}_f, \boldsymbol{d}_\tau \in \mathbb{R}^3$ are the external disturbance force and torque. The external disturbances mainly include the forces and moments caused by non-spherical Earth, atmospheric drag, lunisolar gravitational perturbation and solar radiation pressure. $\boldsymbol{J} \in \mathbb{R}^{3\times3}$ is the inertia matrix of the spacecraft.

Remark 1: As per the Euler theorem, the relative attitude between two coordinate systems can be described by rotating around an axis $\boldsymbol{X} = [X_1, X_2, X_3]^T$ by a certain angle Φ. There exists a relationship between MRPs and the vector $\boldsymbol{X}$, given by $\boldsymbol{\sigma} = \boldsymbol{X}\, tan\frac{\Phi}{4}$. The MRPs become singular when $\Phi = \pm 2\pi$ rad. However, when $\boldsymbol{\sigma}^T\boldsymbol{\sigma} > 1$, the original MRPs σ can be switched to its shadow set $\boldsymbol{\sigma}^s = -\boldsymbol{\sigma}/\boldsymbol{\sigma}^T\boldsymbol{\sigma}$ to ensure a non-singular global attitude rotation. In this paper, to avoid using shadow sets and simplify the derivation of attitude, the range of motion for Euler angles Φ is $[-\pi, \pi]$, which guarantees $\boldsymbol{\sigma}^T\boldsymbol{\sigma} \leq 1$ at all times [36].

https://doi.org/10.1017/aer.2024.2 Published online by Cambridge University Press

During spacecraft operations, the mass and moment of inertia usually have uncertainties. The actual values are typically composed of the nominal values and uncertainties, expressed as $m = m_o + \Delta m$ and $\boldsymbol{J} = \boldsymbol{J}_o + \boldsymbol{\Delta J}$, respectively. Here, m_o and $\boldsymbol{J}_o$ represent the nominal values of the mass and moment of inertia matrices. Δm represents the mass uncertainty caused by fuel consumption, while $\boldsymbol{\Delta} J$ is the uncertainty of the moment of inertia caused by the displacement of the centre of mass and the expansion and contraction of solar panels. To simplify equation derivation, when representing the inverse matrix of mass and moment of inertia, the influence caused by parameter uncertainty makes it expressed as two parts. Then, we can define $m^{-1} \triangleq {m_o}^{-1} + \Delta m^{-1}$, $\boldsymbol{J}^{-1} \triangleq \boldsymbol{J_o}^{-1} + \Delta \boldsymbol{J}^{-1}$ [24]. Combined with Equation (2), the 6-DOF dynamical system with external disturbance and parameter uncertainties is [24]

$$\begin{aligned}
\ddot{\boldsymbol{r}} &= -\mu \boldsymbol{r} + m_o^{-1} \boldsymbol{f} + \Delta m^{-1} \boldsymbol{f} + m^{-1} \boldsymbol{d}_f, \\
\ddot{\boldsymbol{\sigma}} &= \dot{G}(\boldsymbol{\sigma})\, \boldsymbol{w} - G(\boldsymbol{\sigma})\, {\boldsymbol{J}_o}^{-1} \psi(\boldsymbol{w})\, \boldsymbol{J}_o \boldsymbol{w} + G(\boldsymbol{\sigma})\, \boldsymbol{J}_o^{-1} \tau + G(\boldsymbol{\sigma})\, \boldsymbol{\Delta J}^{-1} \tau \\
&\quad - G(\boldsymbol{\sigma})\, \boldsymbol{\Delta J}^{-1} \psi(\boldsymbol{w})\, \boldsymbol{J} \boldsymbol{w} - G(\boldsymbol{\sigma})\, \boldsymbol{J}_o^{-1} \psi(\boldsymbol{w})\, \boldsymbol{\Delta J} \boldsymbol{w} + G(\boldsymbol{\sigma})\, \boldsymbol{J}^{-1} \boldsymbol{d}_\tau
\end{aligned} \tag{3}$$

2.3.2 Spacecraft tracking error dynamics

The attitude error and the rotation matrix are [37]

$$\begin{cases}
\boldsymbol{\sigma}_e = \frac{\sigma_t(\boldsymbol{\sigma}^T \boldsymbol{\sigma} - 1) + \boldsymbol{\sigma}(1 - \boldsymbol{\sigma}_t^T \boldsymbol{\sigma}_t) - 2\psi(\boldsymbol{\sigma}_t)\boldsymbol{\sigma}}{1 + \boldsymbol{\sigma}_t{}^T \boldsymbol{\sigma}_t \boldsymbol{\sigma}^T \boldsymbol{\sigma} + 2\boldsymbol{\sigma}_t{}^T \boldsymbol{\sigma}} \\
T(\boldsymbol{\sigma}_e) = \frac{8}{(1 + \boldsymbol{\sigma}_e^T \boldsymbol{\sigma}_e)^2} \psi^2(\boldsymbol{\sigma}_e) - \frac{4(1 - \boldsymbol{\sigma}_e^T \boldsymbol{\sigma}_e)}{(1 + \boldsymbol{\sigma}_e^T \boldsymbol{\sigma}_e)^2} \psi(\boldsymbol{\sigma}_e) + I_3
\end{cases} \tag{4}$$

By the way, there are

$$\begin{cases}
\dot{\boldsymbol{\sigma}}_e = G(\boldsymbol{\sigma}_e)\, \boldsymbol{w}_e \\
\boldsymbol{w}_e = \boldsymbol{w} - T(\boldsymbol{\sigma}_e) \boldsymbol{w}_t
\end{cases} \tag{5}$$

and

$$\dot{T} = -\psi(\boldsymbol{w}_e)\, T \tag{6}$$

Then, the 6-DOF tracking error dynamics with external disturbance and parameter uncertainties can be expressed as a second-order tracking error dynamic equation

$$\begin{aligned}
\ddot{\boldsymbol{r}}_e &= -\mu \boldsymbol{r} - \ddot{\boldsymbol{r}}_t + m_o^{-1} \boldsymbol{f} + \Delta m^{-1} \boldsymbol{f} + m^{-1} \boldsymbol{d}_f, \\
\ddot{\boldsymbol{\sigma}}_e &= \dot{G}(\boldsymbol{\sigma}_e)\, \boldsymbol{w}_e - G(\boldsymbol{\sigma}_e)\, \boldsymbol{J}_o^{-1} \psi(\boldsymbol{w})\, \boldsymbol{J}_o \boldsymbol{w} + G(\boldsymbol{\sigma}_e)\, \psi(\boldsymbol{w}_e)\, T(\boldsymbol{\sigma}_e)\, \boldsymbol{w}_t + G(\boldsymbol{\sigma}_e)\, \boldsymbol{J}_o^{-1} \tau \\
&\quad - G(\boldsymbol{\sigma}_e)\, \boldsymbol{\Delta} J^{-1} \psi(\boldsymbol{w})\, \boldsymbol{J} \boldsymbol{w} - G(\boldsymbol{\sigma}_e)\, \boldsymbol{J}_o^{-1} \psi(\boldsymbol{w})\, \boldsymbol{\Delta J} \boldsymbol{w} + G(\boldsymbol{\sigma}_e)\, \boldsymbol{\Delta J}^{-1} \boldsymbol{\tau} + G(\boldsymbol{\sigma}_e)\, \boldsymbol{J}^{-1} \boldsymbol{d}_\tau
\end{aligned} \tag{7}$$

The first derivative of $G(\boldsymbol{\sigma}_e)$ is

$$\dot{G}(\boldsymbol{\sigma}_e) = \frac{1}{4} \left[-2\boldsymbol{\sigma}_e^T \dot{\boldsymbol{\sigma}}_e \boldsymbol{I}_3 + 2\psi(\dot{\boldsymbol{\sigma}}_e) + 2\dot{\boldsymbol{\sigma}}_e \boldsymbol{\sigma}_e{}^T + 2\boldsymbol{\sigma}_e \dot{\boldsymbol{\sigma}}_e{}^T \right] \tag{8}$$

Thus, the 6-DOF model can be expressed as

$$\begin{aligned}
\ddot{\boldsymbol{r}}_e &= \boldsymbol{h}_b + m_o^{-1} \boldsymbol{f} + \boldsymbol{d}_b, \\
\ddot{\boldsymbol{\sigma}}_e &= \boldsymbol{h}_a + G(\boldsymbol{\sigma}_e)\, {\boldsymbol{J}_o}^{-1} \boldsymbol{\tau} + \boldsymbol{d}_a
\end{aligned} \tag{9}$$

where

$$\begin{aligned}
\boldsymbol{h}_b &= -\mu \boldsymbol{r} - \ddot{\boldsymbol{r}}_t, \\
\boldsymbol{d}_b &= \Delta m^{-1} \boldsymbol{f} + m^{-1} \boldsymbol{d}_f, \\
\boldsymbol{h}_a &= \dot{G}(\boldsymbol{\sigma}_e)\, \boldsymbol{w}_e - G(\boldsymbol{\sigma}_e)\, \boldsymbol{J}_o^{-1} \psi(\boldsymbol{w})\, \boldsymbol{J}_o \boldsymbol{w} + G(\boldsymbol{\sigma}_e)\, \psi(\boldsymbol{w}_e)\, T(\boldsymbol{\sigma}_e)\, \boldsymbol{w}_t, \\
\boldsymbol{d}_a &= -G(\boldsymbol{\sigma}_e)\, \boldsymbol{\Delta J}^{-1} \psi(\boldsymbol{w})\, \boldsymbol{J} \boldsymbol{w} - G(\boldsymbol{\sigma}_e)\, \boldsymbol{J}_o^{-1} \psi(\boldsymbol{w})\, \boldsymbol{\Delta} J w + G(\boldsymbol{\sigma}_e)\, \boldsymbol{\Delta J}^{-1} \tau + G(\boldsymbol{\sigma}_e)\, \boldsymbol{J}^{-1} \boldsymbol{d}_\tau
\end{aligned} \tag{10}$$

https://doi.org/10.1017/aer.2024.2 Published online by Cambridge University Press

Let $\boldsymbol{e_1} = [\boldsymbol{r_e}^T, \boldsymbol{\sigma_e}^T]^T$ and $\boldsymbol{e_2} = [\boldsymbol{v_e}^T, \boldsymbol{w_e}^T]^T$. The 6-DOF tracking error dynamics with parameter uncertainties and external disturbance can be formulated as

$$\begin{aligned} \dot{\boldsymbol{e}}_1 &= \boldsymbol{e_2}, \\ \dot{\boldsymbol{e}}_2 &= \boldsymbol{h} + \boldsymbol{M_C}\boldsymbol{u} + \boldsymbol{d} \end{aligned} \tag{11}$$

where $\boldsymbol{h} = [\boldsymbol{h_b}^T, \boldsymbol{h_a}^T]^T$ is the inherent nonlinearity of the system. $\boldsymbol{u} = [\boldsymbol{f}^T, \boldsymbol{\tau}^T]^T$ is the control input and $\boldsymbol{u} = [u_1, u_2, \ldots, u_6]^T$. $\boldsymbol{d} = [\boldsymbol{d_b}^T, \boldsymbol{d_a}^T]^T$ is the lumped disturbance term, including external disturbance and parameter uncertainties. $\boldsymbol{M_C}$ is

$$\boldsymbol{M_C} = \begin{bmatrix} m_o^{-1} I_3 & O_3 \\ O_3 & G(\boldsymbol{\sigma_e})\, \boldsymbol{J_o}^{-1} \end{bmatrix} \tag{12}$$

The input saturation of the spacecraft system is

$$u_k = \mathrm{sat}(u_{ik}) = \begin{cases} \mathrm{sign}(u_{ik})\, u_{ik\max}, & |u_{ik}| \geq u_{ik\max} \\ u_{ik}, & |u_{ik}| < u_{ik\max} \end{cases} \quad k = 1, 2, 3 \ldots 6. \tag{13}$$

where $\boldsymbol{u_i}$ is the actual controller output, $u_{ik\max}$ is the bound of u_{ik} and $u_{ik\max} > 0$.

Before designing the observer and controller, there are two points to note.

(1) The modeling and control problems of the spacecraft tracking mission discussed in this paper are conducted in the continuous-time domain. The position and attitude of a controlled spacecraft can be accurately measured through onboard sensors. Since the measurement signals from various onboard sensors are usually filtered, this paper assumes that the state and its uncertainty are second-order differentiable [5]. Moreover, the characteristics of the spacecraft (such as shape and mass) change slowly over time due to fuel consumption and vibrations [4]. Therefore, the derivatives of mass uncertainty and moment of inertia uncertainty are bounded, meaning they are Lipschitz continuous.

(2) The disturbance forces acting on the spacecraft mainly include Earth oblateness perturbation, atmospheric drag perturbation, solar radiation pressure perturbation and the perturbation from the third-body gravitation. The main disturbance torques include gravity gradient torque, aerodynamic torque, solar radiation torque and magnetic torque [24]. These disturbances forces and torques change slowly over time. Thus, they are assumed to be Lipschitz continuous [4]. In other words, disturbance forces and torques can be differentiated, and their differential values have an upper bound.

Based on the above two points, the following assumptions can be made.

Assumption 1. *The spacecraft's dynamical system is detectable and can be stabilised [38].*

Assumption 2. *The parameter uncertainties Δm and $\boldsymbol{\Delta J}$ are bounded and satisfy $|\Delta m| \leq \Delta \bar{m}$ and $\|\boldsymbol{\Delta J}\| \leq \Delta \bar{J}$, where $\Delta \bar{m}$ and $\Delta \bar{J}$ are nonnegative constants. The disturbance force and torque $\boldsymbol{d_f}, \boldsymbol{d_\tau} \in \mathbb{R}^3$ are bounded. The lumped disturbance $\boldsymbol{d}$ is bounded, and its derivative satisfies $||\dot{\boldsymbol{d}}|| \leq \delta d$, where δd is a nonnegative constant.*

Assumptions 1 and 2 mean that the spacecraft system is controllable and observable. It is reasonable because spacecraft always install enough sensors and actuators to provide enough measurement of control force and torque. These two assumptions make it possible to design the corresponding controller and observer of the spacecraft system.

https://doi.org/10.1017/aer.2024.2 Published online by Cambridge University Press

3.0 Fixed-time disturbance observer design

3.1 Modified lumped disturbance

Due to the physical limitations, the actuator exhibits a saturation phenomenon. Input saturation nonlinearity will reduce the system performance and even break the stability of the closed-loop system. Therefore, the influence of input saturation should be considered in the controller design. An auxiliary variable is introduced in this section to represent the input overshoot. The adverse effects are directly transformed into a lumped disturbance. The fixed-time disturbance observer is designed to suppress the lumped disturbance, including parameter uncertainties, external disturbance and input saturation. Compared with the traditional method of adding an anti-saturation structure, the system structure of this method will be concise.

In the input saturation formula (13), when $u_{ik} = u_{ik\max}(k = 1, 2 \ldots 6)$, there is a sharp corner, which makes the output of the actuator have strong nonlinearity. To avoid this strong nonlinearity, a smooth function is used to approximate the input saturation function [39]

$$\mathrm{sat}(u_{ik}) \approx u_{ik\max} \cdot \tanh\left(\frac{u_{ik}}{u_{ik\max}}\right) \tag{14}$$

Furthermore, define an auxiliary variable $\boldsymbol{\Delta u} = [\Delta u_1, \Delta u_2, \cdots, \Delta u_6]^T$, with

$$\Delta u_k = \mathrm{sat}(u_{ik}) - u_{ik}, k = 1, 2, 3 \ldots 6 \tag{15}$$

Equations (14) and (15) yield to $\mathrm{sat}(\boldsymbol{u_i}) = \boldsymbol{u_i} + \boldsymbol{\Delta u}$. Then replace $\boldsymbol{u}$ in Equation (11) with $\mathrm{sat}(\boldsymbol{u})$, and the tracking error system can be rewritten as

$$\begin{aligned} \dot{\boldsymbol{e}}_1 &= \boldsymbol{e}_2, \\ \dot{\boldsymbol{e}}_2 &= \boldsymbol{h} + \boldsymbol{M}_c \mathrm{sat}(\boldsymbol{u}_i) + \bar{\boldsymbol{d}} = \boldsymbol{h} + \boldsymbol{M}_c \boldsymbol{u} + \boldsymbol{M}_c \boldsymbol{\Delta u} + \bar{\boldsymbol{d}} \end{aligned} \tag{16}$$

where $\bar{\boldsymbol{d}} = [\bar{\boldsymbol{d}}_b{}^T, \bar{\boldsymbol{d}}_a{}^T]^T$ and

$$\begin{aligned} \bar{\boldsymbol{d}}_b &= \Delta m^{-1} \mathrm{sat}(\boldsymbol{f}) + m^{-1} \boldsymbol{d}_f, \\ \bar{\boldsymbol{d}}_a &= -G(\boldsymbol{\sigma}_e)\, \boldsymbol{\Delta J}^{-1} \psi(\boldsymbol{w})\, \boldsymbol{J w} - G(\boldsymbol{\sigma}_e)\, \boldsymbol{J}_o^{-1} \psi(\boldsymbol{w})\, \boldsymbol{\Delta J w} + G(\boldsymbol{\sigma}_e)\, \boldsymbol{\Delta J}^{-1} \mathrm{sat}(\boldsymbol{\tau}) + G(\boldsymbol{\sigma}_e)\, \boldsymbol{J}^{-1} \boldsymbol{d}_\tau \end{aligned} \tag{17}$$

Define $\boldsymbol{d}_s = \boldsymbol{M}_c \boldsymbol{\Delta u} + \bar{\boldsymbol{d}}$. The modified lumped disturbance $\boldsymbol{d}_s$ is bounded. Since $\mathrm{sat}(\boldsymbol{u_i}) = \boldsymbol{u_i} + \boldsymbol{\Delta u}$, $\boldsymbol{d}_s = \boldsymbol{M}_c \boldsymbol{\Delta u} + \bar{\boldsymbol{d}}$, $\boldsymbol{d}_s = \boldsymbol{M}_c[\mathrm{sat}(\boldsymbol{u_i}) - \boldsymbol{u_i}] + \bar{\boldsymbol{d}}$ and $\dot{\boldsymbol{d}}_s = \dot{\boldsymbol{M}}_c[\mathrm{sat}(\boldsymbol{u_i}) - \boldsymbol{u_i}] + \boldsymbol{M}_c[\mathrm{sat}(\dot{\boldsymbol{u}}_i) - \dot{\boldsymbol{u}}_i] + \dot{\bar{\boldsymbol{d}}}$ hold. The system is controllable, so the control input u is bounded. Since a smooth function replaces the traditional saturation function, $\mathrm{sat}(\boldsymbol{u_i})$ and $sat(\dot{\boldsymbol{u}}_i)$ are bounded. In addition, since the uncertain parameters Δm and $\boldsymbol{\Delta J}$ and the external disturbance $\boldsymbol{d}_f$ and $\boldsymbol{d}_\tau$ are bounded, we can know $\boldsymbol{d}_s$ and $\dot{\boldsymbol{d}}_s$ are bounded. Therefore, $\boldsymbol{d}_s$ is bounded, and its derivative satisfies $||\dot{\boldsymbol{d}}_s|| \leq \delta d_s$, where δd_s is a nonnegative constant.

3.2 FT-DO design

In this section, an FT-DO with fewer parameters is proposed for estimating the modified lumped disturbances. The convergence of the estimation error subsystem does not depend on the initial state of the system. First of all, introduce the following lemma.

Lemma 1. *[34] For the following dynamical system (18) with a bounded disturbance $\boldsymbol{\xi}(t)$, both state vectors $\boldsymbol{x}(t)$ and $\boldsymbol{y}(t)$ converge to the origin uniformly in a fixed time T_f calculated by Equation (19).*

$$\begin{aligned} \dot{\boldsymbol{x}}(t) &= -\lambda_1 \frac{\boldsymbol{x}(t)}{\|\boldsymbol{x}(t)\|^{\frac{1}{2}}} - \lambda_2 \boldsymbol{x}(t)\, ||\boldsymbol{x}(t)||^{p-1} + \boldsymbol{y}(t) \\ \dot{\boldsymbol{y}}(t) &= -\ell \frac{\boldsymbol{x}(t)}{\|\boldsymbol{x}(t)\|} + \boldsymbol{\xi}(t) \end{aligned} \tag{18}$$

https://doi.org/10.1017/aer.2024.2 Published online by Cambridge University Press

$$T_f \leq \left(\frac{1}{\lambda_2 (p-1)\, \varpi^{p-1}} + \frac{2\left(\sqrt{n}\varpi\right)^{1/2}}{\lambda_1}\right)\left(1 + \frac{M}{m\left(1-\sqrt{2\ell}/\lambda_1\right)}\right) \tag{19}$$

where n is the dimension of the state vector. The parameters satisfy $\varpi > 0$, $\lambda_1, \lambda_2, \ell > 0$, *and the bound of* $\|\boldsymbol{\xi}(t)\|$ *is L. The relationships* $M = \ell + L, m = \ell - L, \ell > 4L$, *and* $\lambda_1 > \sqrt{2\ell}$ *hold.*

The state vector of the observer is defined as $\boldsymbol{\vartheta} = [\boldsymbol{\vartheta_1}^T, \boldsymbol{\vartheta_2}^T]^T$, where $\boldsymbol{\vartheta_1}, \boldsymbol{\vartheta_2} \in \mathbb{R}^6$. The fixed-time disturbance observer can be expressed as

$$\begin{aligned}
\dot{\boldsymbol{\vartheta}}_1 &= -\lambda_1 \frac{\boldsymbol{e_{o1}}}{\|e_{o1}\|^{1/2}} - \lambda_2(\boldsymbol{\vartheta_1} - \boldsymbol{e_2})\, ||\boldsymbol{\vartheta_1} - \boldsymbol{e_2}||^{p-1} + \boldsymbol{\vartheta_2} + \boldsymbol{h} + \boldsymbol{M_c u} \\
\dot{\boldsymbol{\vartheta}}_2 &= -\lambda_3 \frac{\boldsymbol{e_{o1}}}{\|e_{o1}\|}
\end{aligned} \tag{20}$$

where $\boldsymbol{e_{o1}} = \boldsymbol{\vartheta_1} - \boldsymbol{e_2}$, $\boldsymbol{e_{o2}} = \boldsymbol{\vartheta_2} - \boldsymbol{d}_s$, and they are estimated errors, $p \in \mathbb{R}$ and $p > 1$. The parameters $\lambda_1, \lambda_2, \lambda_3$ satisfy $\lambda_1 > \sqrt{2\lambda_3}$, $\lambda_2 > 0$, and $\lambda_3 > \delta d_s$, where δd_s is the bound of $||\dot{\boldsymbol{d}}_s||$.

Theorem 1. *For the tracking error dynamical system (16), the estimation errors* $\boldsymbol{e_{o1}}$ *and* $\boldsymbol{e_{o2}}$ *will converge to the origin within a fixed time by employing the disturbance observer (20), and the modified lumped disturbance* $\boldsymbol{d}_s$ *can be estimated by* $\boldsymbol{\vartheta_2}$.

Proof. Since $\boldsymbol{e_{o1}} = \boldsymbol{\vartheta_1} - \boldsymbol{e_2}$ and $\boldsymbol{e_{o2}} = \boldsymbol{\vartheta_2} - \boldsymbol{d}_s$, combining Equations (16) and (20), $\dot{\boldsymbol{e}}_{o1}$ can be derived as follows

$$\dot{\boldsymbol{e}}_{o1} = -\lambda_1 \frac{\boldsymbol{e_{o1}}}{||\boldsymbol{e_{o1}}||^{1/2}} - \lambda_2 \boldsymbol{e_{o1}} ||\boldsymbol{e_{o1}}||^{p-1} + \boldsymbol{e_{o2}} \tag{21}$$

Taking the derivative of $\boldsymbol{e}_{o2}$, the estimated error dynamics can be established as

$$\begin{aligned}
\dot{\boldsymbol{e}}_{o1} &= -\lambda_1 \frac{\boldsymbol{e_{o1}}}{||\boldsymbol{e_{o1}}||^{1/2}} - \lambda_2 \boldsymbol{e_{o1}} ||\boldsymbol{e_{o1}}||^{p-1} + \boldsymbol{e_{o2}} \\
\dot{\boldsymbol{e}}_{o2} &= -\lambda_3 \frac{\boldsymbol{e_{o1}}}{||\boldsymbol{e_{o1}}||} - \dot{\boldsymbol{d}}_s
\end{aligned} \tag{22}$$

According to Lemma 1, the state vectors $\boldsymbol{e}_{o1}$ and $\boldsymbol{e}_{o2}$ of the estimated error dynamical system (22) with a bounded disturbance $\boldsymbol{d}_s$ will uniformly converge to the origin within a fixed time T_o.

$$T_o \leq \left(\frac{1}{\lambda_2 (p-1)\, \varsigma^{p-1}} + \frac{2(\sqrt{6}\varsigma)^{1/2}}{\lambda_1}\right)\left(1 + \frac{\lambda_3 + \delta d}{(\lambda_3 - \delta d)\left(1 - 2\sqrt{\lambda_3}/\lambda_1\right)}\right) \tag{23}$$

where ς is a small constant. When $\varsigma = (6^{1/4}\lambda_1/\lambda_2)^{1/(p+0.5)}$, the upper bound of T_o is minimised. Therefore, the lumped disturbance $\boldsymbol{d}_s$ can be estimated by $\boldsymbol{\vartheta_2}$ within a fixed time. □

The designed FT-DO can observe various complex disturbances. Especially in this paper, the modified lumped disturbance includes the adverse effects caused by input saturation. The FT-DO designed in this paper can still suppress this lumped disturbance. Compared with the traditional anti-saturation scheme (Fig. 1), the design of the FT-DO avoids adding additional sub-dynamics to the system, making the control system structure concise.

https://doi.org/10.1017/aer.2024.2 Published online by Cambridge University Press

4.0 Fixed-time non-singular terminal sliding mode controller design

In this section, for 6-DOF tracking control of the spacecraft, an FT-NTSM controller is proposed. The purpose is to make the tracking error system (16) converge to the neighbourhood of zero within a fixed time. The following lemmas are introduced.

Lemma 2. *[22] For any real numbers $\chi_1, \chi_2, \ldots, \chi_n$ and a constant $\iota > 0$, the following inequalities hold.*

$$\begin{cases} |\chi_1|^{\iota} + |\chi_2|^{\iota} + \ldots + |\chi_n|^{\iota} \geq \left(\sum_{i=1}^{n} |\chi_i|\right)^{\iota}, 0 < \iota \leq 1 \\ |\chi_1|^{\iota} + |\chi_2|^{\iota} + \ldots + |\chi_n|^{\iota} \geq n^{1-\iota}\left(\sum_{i=1}^{n} |\chi_i|\right)^{\iota}, \iota \geq 1 \end{cases} \tag{24}$$

Lemma 3. *[21] Consider the nonlinear system*

$$\dot{\boldsymbol{\chi}}(t) = \boldsymbol{g}(\boldsymbol{\chi}(t)), \boldsymbol{\chi}(0) = \boldsymbol{0}, \boldsymbol{g}(\boldsymbol{0}) = \boldsymbol{0}, \boldsymbol{\chi} \in \mathbb{R}^n \tag{25}$$

where $\boldsymbol{g}: U_0 \to \mathbb{R}^n$ is continuous in an open neighbourhood U_0 of the origin. The unique solution of system (25) is supposed to exist for any initial conditions. For the nonlinear system (25), if there exists a Lyapunov function $V(\boldsymbol{\chi})$ and scalars $0 < p < 1$, $g > 1$, $\beta > 0, \alpha > 0, 0 < \delta < \infty$, such that $\dot{V}(\boldsymbol{\chi}) \leq -\beta V^p(\boldsymbol{\chi}) - \alpha V^g(\boldsymbol{\chi}) + \delta$ holds, the trajectory of this system is practical fixed-time stable. Moreover, the residual set of the solution of system (25) can be given by $\left\{\lim_{t \to T} \boldsymbol{\chi} | V(\boldsymbol{\chi}) \leq min\left\{\beta^{-1/p}\left(\frac{\delta}{1-\theta}\right)^{\frac{1}{p}}, \alpha^{-1/p}\left(\frac{\delta}{1-\theta}\right)^{\frac{1}{g}}\right\}\right\}$, where θ is a scalar and satisfies $0 < \theta \leq 1$. The time to reach the residual set is bounded by $T \leq (1/\beta\theta(1-p)) + (1/\alpha\theta(g-1))$.

4.1 FT-NTSM controller design

Since the design of the sliding mode surface is based on the phase plane, the position and attitude tracking error vector $\boldsymbol{e_1} = [e_{11}, e_{12}, \ldots, e_{16}]^T$ and its first-order derivative $\boldsymbol{e_2} = [e_{21}, e_{22}, \ldots, e_{26}]^T$ are selected as state variables to construct the phase plane. The parameters p_k,q_k,m_k and n_k,$(k = 1, 2)$ are positive odd integers and satisfy $p_1 < q_1 < 2p_1$,$p_2 < q_2$, $m_k > n_k$ and $\frac{m_1}{n_1} - \frac{p_1}{q_1} > 1$. In order to avoid singularity, inspired by [19], the non-singular terminal sliding mode surface s is designed as

$$\boldsymbol{s} = \boldsymbol{e_1} + [\boldsymbol{\kappa}(\boldsymbol{e_1}) \cdot \boldsymbol{e_2}]^{\frac{q_1}{p_1}} \tag{26}$$

where $s = [s_1, s_2, \cdots, s_6]^T$. $\boldsymbol{\kappa} \in \mathbb{R}^{6\times 6}$ is a diagonal matrix. Its diagonal element $\kappa_k(\kappa_k: \mathbb{R} \to \mathbb{R}^+, k = 1, \ldots 6)$ is a scalar positive function and can be expressed as

$$\kappa_k(e_{1k}) = \frac{1}{\nu_1 e_{1k}^{\frac{m_1}{n_1} - \frac{p_1}{q_1}} + \eta_1}, k = 1, 2 \ldots 6 \tag{27}$$

where $\nu_1 > 0$ and $\eta_1 > 0$. Combined with the disturbance observer, the first derivative of the sliding mode surface is

$$\begin{aligned} \dot{s} = \frac{q_1}{p_1}\Big[\boldsymbol{\kappa} \cdot \boldsymbol{e_2}\Big]^{\frac{q_1}{p_1}-1}\Big[- \nu_1\left(\frac{m_1}{n_1} - \frac{p_1}{q_1}\right) \mathrm{diag}(\boldsymbol{e_1})^{\frac{m_1}{n_1} - \frac{p_1}{q_1} - 1}\boldsymbol{\kappa}^2 \mathrm{diag}(\boldsymbol{e_2})\, \boldsymbol{e_2} \\ + \boldsymbol{\kappa}(\boldsymbol{h} + \boldsymbol{M_C}\boldsymbol{u} + \boldsymbol{d}_s)\Big] + \boldsymbol{e_2} \end{aligned} \tag{28}$$

Considering all the possibilities of the initial state of the spacecraft error system, the fixed-time non-singular control law base on FT-DO can be expressed as

$$\begin{cases} \boldsymbol{u} = (\boldsymbol{M_C}\boldsymbol{\kappa})^{-1}\left[\nu_1(\frac{m_1}{n_1} - \frac{p_1}{q_1})\mathrm{diag}(\boldsymbol{e_1})^{\frac{m_1}{n_1} - \frac{p_1}{q_1} - 1}\boldsymbol{\kappa}^2 \mathrm{diag}(\boldsymbol{e_2})\boldsymbol{e_2} - \frac{p_1}{q_1}\boldsymbol{\kappa}^{1-\frac{q_1}{p_1}}\boldsymbol{e_2}^{2-\frac{q_1}{p_1}}\right] \\ \quad - \boldsymbol{M_C}^{-1}(\boldsymbol{h} + \hat{\boldsymbol{d}}_s + \gamma \mathrm{sign}(\boldsymbol{s})) - \boldsymbol{M_C}^{-1}\frac{p_1}{q_1}\boldsymbol{\kappa}^{-\frac{q_1}{p_1}}\boldsymbol{e_2}^{1-\frac{q_1}{p_1}}\mathrm{diag}(\boldsymbol{\phi_\tau})(\nu_2 \boldsymbol{s}^{\frac{m_2}{n_2}} + \eta_2 \boldsymbol{s}^{\frac{p_2}{q_2}}), \quad \boldsymbol{e_2}(0) \neq \boldsymbol{0} \\ \boldsymbol{u} = -\boldsymbol{M_C}^{-1}(\boldsymbol{h} + \hat{\boldsymbol{d}}_s + \gamma \mathrm{sign}(\boldsymbol{s})) - \boldsymbol{M_C}^{-1}\frac{p_1}{q_1}\boldsymbol{\kappa}^{-\frac{q_1}{p_1}}(\nu_2 \boldsymbol{s}^{\frac{m_2}{n_2}} + \eta_2 \boldsymbol{s}^{\frac{p_2}{q_2}}), \quad \boldsymbol{e_2}(0) = \boldsymbol{0} \end{cases} \tag{29}$$

https://doi.org/10.1017/aer.2024.2 Published online by Cambridge University Press

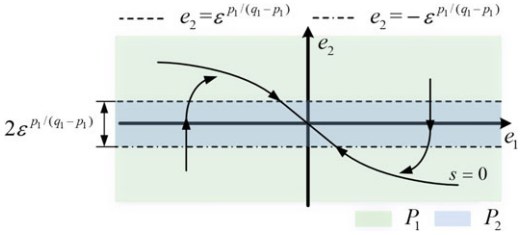

Figure 4. *The phase plane diagram of the system.*

where γ ($\gamma > \|\boldsymbol{e_{o2}}\|$) is the designed switching gain, and the parameters satisfy $\nu_2 > 0$ and $\eta_2 > 0$. $\hat{\boldsymbol{d}}_s$ ($\hat{\boldsymbol{d}}_s = \hat{\boldsymbol{\vartheta}}_2$) denotes the estimated value of $\boldsymbol{d}_s$. Due to $1 < \frac{q_1}{p_1} < 2$, the nonlinear function $\phi_{\tau k}(\cdot) : [0, +\infty) \to [0, 1]$ is introduced to avoid the singularity of $\boldsymbol{e_2}^{1-\frac{q_1}{p_1}}$ in (29). $\boldsymbol{\phi_\tau} = [\phi_{\tau 1}, \phi_{\tau 2}, \cdots \phi_{\tau k}]^T (k = 1, 2 \ldots 6)$, and $\phi_{\tau k}$ is given by

$$\phi_{\tau k}(f_k) = \begin{cases} \sin\left(\frac{\pi f_k}{2\varepsilon}\right) & , f_k \leqslant \varepsilon \\ 1 & , f_k > \varepsilon \end{cases} \tag{30}$$

where $f_k = |e_{2k}|^{\frac{q_1}{p_1}-1}$, and ε is a positive constant.

4.2 System stability analysis

Theorem 2. *For the tracking error dynamical system (16), if the FT-DO (20) and the FT-NTSM controller (29) are designed, the state of the tracking error system (16) can converge to the neighbourhood of zero within a fixed time.*

Proof. The candidate Lyapunov function for the entire system is defined as

$$V = \tfrac{1}{2}\boldsymbol{e_{o2}}^T\boldsymbol{e_{o2}} + \tfrac{1}{2}\boldsymbol{s}^T\boldsymbol{s} \tag{31}$$

To facilitate subsequent derivations, we denote the term $\frac{1}{2}\boldsymbol{e_{o2}}^T\boldsymbol{e_{o2}}$ as V_1 and the term $\frac{1}{2}\boldsymbol{s}^T\boldsymbol{s}$ as V_2. The derivative of V is

$$\dot{V} = \dot{V}_1 + \dot{V}_2 \tag{32}$$

For $\dot{V}_1$, the following inequality holds.

$$\dot{V}_1 = \boldsymbol{e_{o2}}^T\dot{\boldsymbol{e}}_{\boldsymbol{o2}} \leq \left\|\boldsymbol{e_{o2}}^T\dot{\boldsymbol{e}}_{\boldsymbol{o2}}\right\| = \left\|\boldsymbol{e_{o2}}^T\right\| \left\|\lambda_3\frac{\boldsymbol{e_{o1}}}{\boldsymbol{e_{o1}}} + \dot{\boldsymbol{d}}_s\right\| \leq \lambda_3 \|\boldsymbol{e_{o2}}\| + \left\|\boldsymbol{e_{o2}}^T\right\| \|\delta d_s\| \tag{33}$$

Substituting the controller $u(\boldsymbol{e_2}(0) \neq 0)$ in (29) into $\dot{\boldsymbol{s}}$ yields

$$\begin{aligned}\dot{V}_2 &= \boldsymbol{s}^T\dot{\boldsymbol{s}} \\ &= -\nu_2\left(\sum_{k=1}^{n}\left(\phi_{\tau k}(|s_k|)^{\frac{m_2+n_2}{n_2}}\right)\right) - \eta_2\left(\sum_{k=1}^{n}\left(\phi_{\tau k}(|s_k|)^{\frac{p_2+q_2}{q_2}}\right)\right) - \boldsymbol{s}^T\left(\frac{q_1}{p_1}\boldsymbol{\kappa}^{\frac{q_1}{p_1}}\boldsymbol{e_2}^{\frac{q_1}{p_1}-1}(\boldsymbol{e_{o2}} + \gamma\,\mathrm{sign}(\boldsymbol{s}))\right)\end{aligned} \tag{34}$$

Since the existence of the sinusoidal function $\phi_{\tau k}$, the phase plane will be divided into two parts: $P_1 = \{(\boldsymbol{e_1}, \boldsymbol{e_2}) | f_k > \varepsilon\}$ and $P_2 = \{(\boldsymbol{e_1}, \boldsymbol{e_2}) | f_k \leq \varepsilon\}$, as shown in Fig. 4.

https://doi.org/10.1017/aer.2024.2 Published online by Cambridge University Press

Part 1: In area P_1, $\phi_{\tau k}=1$. Since $\frac{m_2+n_2}{2n_2}>1$, $\frac{1}{2}<\frac{p_2+q_2}{2q_2}<1$, based on Lemma 2, the following inequality can be obtained.

$$\begin{aligned}\dot{V}_2 &\leqslant \left(\nu_2\left(n^{\frac{n_2-m_2}{2n_2}}\left(\sum_{k=1}^{n}|s_k|^2\right)^{\frac{m_2+n_2}{2n_2}}\right)+\eta_2\left(\sum_{k=1}^{n}\left(|s_k|^2\right)^{\frac{p_2+q_2}{2q_2}}\right)\right)-\boldsymbol{s}^T\left(\frac{q_1}{p_1}\boldsymbol{\kappa}^{\frac{q_1}{p_1}}\boldsymbol{e}_2^{\frac{q_1}{p_1}-1}(\boldsymbol{e_{o2}}+\gamma\,\mathrm{sign}(\boldsymbol{s}))\right)\\ &\leqslant \left(\nu_2\left(n^{\frac{n_2-m_2}{2n_2}}\left(\sum_{k=1}^{n}|s_k|^2\right)^{\frac{m_2+n_2}{2n_2}}\right)+\eta_2\left(\sum_{k=1}^{n}|s_k|^2\right)^{\frac{p_2+q_2}{2q_2}}\right)-\boldsymbol{s}^T\left(\frac{q_1}{p_1}\boldsymbol{\kappa}^{\frac{q_1}{p_1}}\boldsymbol{e}_2^{\frac{q_1}{p_1}-1}(\boldsymbol{e_{o2}}+\gamma\,\mathrm{sign}(\boldsymbol{s}))\right)\\ &=-\left(\nu_2\left(n^{\frac{n_2-m_2}{2n_2}}\cdot 2^{\frac{m_2+n_2}{2n_2}}\left(\frac{1}{2}\sum_{k=1}^{n}|s_k|^2\right)^{\frac{m_2+n_2}{2n_2}}\right)+\eta_2\cdot 2^{\frac{p_2+q_2}{2q_2}}\left(\frac{1}{2}\sum_{k=1}^{n}|s_k|^2\right)^{\frac{p_2+q_2}{2q_2}}\right)\\ &\quad-\boldsymbol{s}^T\left(\frac{q_1}{p_1}\boldsymbol{\kappa}^{\frac{q_1}{p_1}}\boldsymbol{e}_2^{\frac{q_1}{p_1}-1}(\boldsymbol{e_{o2}}+\gamma\,\mathrm{sign}\,(\boldsymbol{s}))\right)\\ &=-\left(n^{\frac{n_2-m_2}{2n_2}}\cdot 2^{\frac{m_2+n_2}{2n_2}}\nu_2(V_2)^{\frac{m_2+n_2}{2n_2}}+2^{\frac{p_2+q_2}{2q_2}}\eta_2(V_2)^{\frac{p_2+q_2}{2q_2}}\right)-\boldsymbol{s}^T\left(\frac{q_1}{p_1}\boldsymbol{\kappa}^{\frac{q_1}{p_1}}\boldsymbol{e}_2^{\frac{q_1}{p_1}-1}(\boldsymbol{e_{o2}}+\gamma\,\mathrm{sign}\,(\boldsymbol{s}))\right)\end{aligned}\tag{35}$$

where $n=6$. Therefore, $\dot{V}$ satisfies

$$\begin{aligned}\dot{V}&=\dot{V}_1+\dot{V}_2\\ &\leq-\left(n^{\frac{n_2-m_2}{2n_2}}\cdot 2^{\frac{m_2+n_2}{2n_2}}\nu_2(V_2)^{\frac{m_2+n_2}{2n_2}}+2^{\frac{p_2+q_2}{2q_2}}\eta_2(V_2)^{\frac{p_2+q_2}{2q_2}}\right)-\boldsymbol{s}^T\left(\frac{q_1}{p_1}\boldsymbol{\kappa}^{\frac{q_1}{p_1}}\boldsymbol{e}_2^{\frac{q_1}{p_1}-1}(\boldsymbol{e_{o2}}+\gamma\,\mathrm{sign}\,(\boldsymbol{s}))\right)\\ &\quad+\lambda_3||\boldsymbol{e_{o2}}||+||\boldsymbol{e_{o2}}^T||\;||\delta d_s||\\ &\leq-n^{\frac{n_2-m_2}{2n_2}}\cdot 2^{\frac{m_2+n_2}{2n_2}}\nu_2(V_2)^{\frac{m_2+n_2}{2n_2}}-2^{\frac{p_2+q_2}{2q_2}}\eta_2(V_2)^{\frac{p_2+q_2}{2q_2}}-n^{\frac{n_2-m_2}{2n_2}}\cdot 2^{\frac{m_2+n_2}{2n_2}}\nu_2(V_1)^{\frac{m_2+n_2}{2n_2}}-2^{\frac{p_2+q_2}{2q_2}}\eta_2(V_1)^{\frac{p_2+q_2}{2q_2}}\\ &\quad+n^{\frac{n_2-m_2}{2n_2}}\cdot 2^{\frac{m_2+n_2}{2n_2}}\nu_2(V_1)^{\frac{m_2+n_2}{2n_2}}+2^{\frac{p_2+q_2}{2q_2}}\eta_2(V_1)^{\frac{p_2+q_2}{2q_2}}+\lambda_3||\boldsymbol{e_{o2}}||+||\boldsymbol{e_{o2}}^T||\;||\delta d_s||\\ &=-n^{\frac{n_2-m_2}{2n_2}}\cdot 2^{\frac{m_2+n_2}{2n_2}}\nu_2\left((V_2)^{\frac{m_2+n_2}{2n_2}}+(V_1)^{\frac{m_2+n_2}{2n_2}}\right)-2^{\frac{p_2+q_2}{2q_2}}\eta_2\left((V_2)^{\frac{p_2+q_2}{2q_2}}+(V_1)^{\frac{p_2+q_2}{2q_2}}\right)\\ &\quad+n^{\frac{n_2-m_2}{2n_2}}\cdot 2^{\frac{m_2+n_2}{2n_2}}\nu_2\left(\frac{1}{2}||\boldsymbol{e_{o2}}||^2\right)^{\frac{m_2+n_2}{2n_2}}+2^{\frac{p_2+q_2}{2q_2}}\eta_2\left(\frac{1}{2}||\boldsymbol{e_{o2}}||^2\right)^{\frac{p_2+q_2}{2q_2}}+\lambda_3||\boldsymbol{e_{o2}}||+||\boldsymbol{e_{o2}}^T||\;||\delta d_s||\end{aligned}\tag{36}$$

Let $\varphi=\nu_3\left(\frac{1}{2}\|\boldsymbol{e_{o2}}\|^2\right)^{\frac{m_2+n_2}{2n_2}}+\eta_3\left(\frac{1}{2}\|\boldsymbol{e_{o2}}\|^2\right)^{\frac{p_2+q_2}{2q_2}}+\lambda_3\|\boldsymbol{e_{o2}}\|+\|\boldsymbol{e_{o2}}^T\|\|\delta d_s\|$, where $\nu_3=n^{\frac{n_2-m_2}{2n_2}}\cdot 2^{\frac{m_2+n_2}{2n_2}}\nu_2$, $\eta_3=2^{\frac{p_2+q_2}{2q_2}}\eta_2$, Equation (36) can be rewritten as

$$\dot{V}\leq-\nu_3\left((V_2)^{\frac{m_2+n_2}{2n_2}}+(V_1)^{\frac{m_2+n_2}{2n_2}}\right)-\eta_3\left((V_2)^{\frac{p_2+q_2}{2q_2}}+(V_1)^{\frac{p_2+q_2}{2q_2}}\right)+\varphi\tag{37}$$

According to Lemma 2, there are $(V_2)^{\frac{m_2+n_2}{2n_2}}+(V_1)^{\frac{m_2+n_2}{2n_2}}\geq 2^{\frac{n_2-m_2}{2n_2}}V^{\frac{m_2+n_2}{2n_2}}$ and $(V_2)^{\frac{p_2+q_2}{2q_2}}+(V_1)^{\frac{p_2+q_2}{2q_2}}\geq V^{\frac{p_2+q_2}{2q_2}}$. Then

$$\dot{V}\leq-\eta_3\left(V^{\frac{p_2+q_2}{2q_2}}\right)-2^{\frac{n_2-m_2}{2n_2}}\nu_3\left(V^{\frac{m_2+n_2}{2n_2}}\right)+\varphi\tag{38}$$

Based on Theorem 1, the estimation error will converge to a small bounded value near zero. Therefore, φ is a small positive number. Let $\nu_4=2^{\frac{n_2-m_2}{2n_2}}\nu_3$, based on Lemma 3, the whole system is fixed-time stable. The convergence time is bounded by

$$T_s\leq\left(1/\left(\nu_4\theta_s\left(\frac{m_2}{n_2}-1\right)\right)\right)+1/\left(\eta_3\theta_s\left(1-\frac{p_2}{q_2}\right)\right)\right)+T_o\tag{39}$$

where $\theta_s\in(0,1)$, and T_o is the convergence time of the observer.

https://doi.org/10.1017/aer.2024.2 Published online by Cambridge University Press

Part 2: In area P_2, there is $0 < \phi_{\tau k} < 1$. When $\boldsymbol{e_2} \neq \boldsymbol{0}$, similar to the steps in Part 1, it is not difficult to prove that $\boldsymbol{s} = \boldsymbol{0}$ is still a domain of attraction. In this part, we need to prove that when $\boldsymbol{e_2} \to \boldsymbol{0}$, only the origin $(\boldsymbol{e_1}, \boldsymbol{e_2}) = (\boldsymbol{0}, \boldsymbol{0})$ is an attractor.

When $\boldsymbol{e_2} \to \boldsymbol{0}$, $\phi_{\tau k} {e_{2k}}^{1-\frac{q_1}{p_1}} \to 1$ holds. The control law is

$$\boldsymbol{u} = -{\boldsymbol{M_C}}^{-1}\left(\boldsymbol{h} + \hat{\boldsymbol{d}}_s + \gamma \operatorname{sign}(\boldsymbol{s})\right) - {\boldsymbol{M_C}}^{-1}\frac{p_1}{q_1}\boldsymbol{\kappa}^{-\frac{q_1}{p_1}}\left(\nu_2 \boldsymbol{s}^{\frac{m_2}{n_2}} + \eta_2 \boldsymbol{s}^{\frac{p_2}{q_2}}\right) \tag{40}$$

Then substitute (40) into $\dot{\boldsymbol{e}}_2$, and we can get

$$\begin{aligned}\dot{\boldsymbol{e}}_2 &= \boldsymbol{d}_s - \hat{\boldsymbol{d}}_s - \gamma \operatorname{sign}(\boldsymbol{s}) - \frac{p_1}{q_1}\boldsymbol{\kappa}^{-\frac{q_1}{p_1}}\left(\nu_2 \boldsymbol{s}^{\frac{m_2}{n_2}} + \eta_2 \boldsymbol{s}^{\frac{p_2}{q_2}}\right) \\ &= -\boldsymbol{e_{o2}} - \gamma \operatorname{sign}(\boldsymbol{s}) - \frac{p_1}{q_1}\boldsymbol{\kappa}^{-\frac{q_1}{p_1}}\left(\nu_2 \boldsymbol{s}^{\frac{m_2}{n_2}} + \eta_2 \boldsymbol{s}^{\frac{p_2}{q_2}}\right)\end{aligned} \tag{41}$$

Since $\gamma > \|\boldsymbol{e_{o2}}\|$, then $\boldsymbol{s} > \boldsymbol{0}, \dot{\boldsymbol{e}}_2 < \boldsymbol{0}$ and $\boldsymbol{s}\ \langle \boldsymbol{0}, \dot{\boldsymbol{e}}_2 \rangle\ \boldsymbol{0}$ hold. Therefore, if $\boldsymbol{e_2}$ is in area P_2, it will increase or decrease monotonically until it leaves area P_2. That is, all states in area P_2 will enter P_1, as shown in Fig. 4. The $\boldsymbol{e_1}$-axis is not an attractor. The crossing time is denoted as $T_\varepsilon(\varepsilon)$, which is very small and can be ignored.

Therefore, for the tracking error dynamics system (16), if the fixed-time disturbance observer (20) and the fixed-time terminal sliding mode controller (29) are designed, the states of the tracking error system can converge to the neighbourhood of zero in a fixed-time bounded by $T_c = T_s + T_\varepsilon$. □

Remark 2: In the selected Lyapunov function (31), the term $\frac{1}{2}\boldsymbol{s}^T\boldsymbol{s}$ ensures the reachability of the sliding surface. The designed control law $\boldsymbol{u}$ guarantees that $\boldsymbol{s}^T * \boldsymbol{s} < 0$ $(\boldsymbol{s} \neq \boldsymbol{0})$ holds, indicating that the tracking error states $\boldsymbol{e_1}$ and $\boldsymbol{e_2}$ will reach the sliding surface and converge towards the equilibrium point along the sliding surface. Furthermore, in addition to the $\frac{1}{2}\boldsymbol{s}^T\boldsymbol{s}$ term, the term $\frac{1}{2}\boldsymbol{e_{o2}}^T\boldsymbol{e_{o2}}$ (note that this term is not the Lyapunov function for the observer error subsystem) is introduced. The purpose of introducing this term is to construct a Lyapunov function in the form of Lemma 3, ensuring fixed-time convergence of the entire system. A similar construction of the Lyapunov function can also be found in the reference [24].

Remark 3: The designed disturbance observer provides feedback compensation for the lumped disturbances $\boldsymbol{d}_s$. Thanks to the disturbance observer's accurate estimation of the lumped disturbance, a smaller switching gain γ can be selected in the controller. Therefore, a small switching gain can ensure the existence of the sliding mode surface. Sliding mode control effectively suppresses disturbances by employing aggressive control gains. The presence of the sign function results in frequent switching of the control signal. Therefore, the larger the controller gain, the more severe the chattering. Consequently, using smaller switching gains helps to reduce system chattering [24].

Remark 4: A nonlinear function ϕ_τ is introduced to avoid the singularity of the controller. Thus, the state space is divided into two regions P_1 and P_2. The transit time T_ε from P_1 to P_2 cannot be estimated precisely. From Fig. 4, it can be seen that the transit time $T_\varepsilon(\varepsilon)$ from the P_2 region to the P_1 region depends on the width of $2\varepsilon^{p_1/(q_1-p_1)}$. This implies that it is possible to select a sufficiently small ε to make $T_\varepsilon(\varepsilon)$ very small. Due to the conservativeness in estimating T_s, it makes sense to ignore the transit time $T_\varepsilon(\varepsilon)$.

5.0 Simulations

5.1 Simulation parameters

For the orbit control of spacecraft, the scenario is set as manoeuvring a circular low Earth orbit spacecraft to another circular orbit within the same orbital plane. In this scenario, adjusting the spacecraft's semi-major axis is sufficient. Therefore, the initial and desired values of the spacecraft's orbital elements $\left[a\,(\mathrm{km}), \bar{e}, i\,(\mathrm{deg}), \Omega\,(\mathrm{deg}), \omega\,(\mathrm{deg}), M_o\,(\mathrm{deg})\right]$ can be set as [7000, 0, 28.5, 100, 0, 130] and [7000.5, 0, 28.5, 100, 0, 130], respectively. Simultaneously, it is also desired for the spacecraft's attitude

https://doi.org/10.1017/aer.2024.2 Published online by Cambridge University Press

Table 1. *The initial tracking errors of orbit and attitude*

Orbit	r_{e1}(m)	r_{e2}(m)	r_{e3}(m)	v_{e1}(rad/s)(m)	v_{e2}(rad/s)(m)	v_{e3}(rad/s)(m)
Initial	275.683	374.962	−182.762	0.1858	−0.1769	−0.0827
Desired	0.00	0.00	0.00	0.00	0.00	0.00
Attitude	σ_{e1}	σ_{e2}	σ_{e3}	w_{e1}(rad/s)	w_{e2}(rad/s)	w_{e3}(rad/s)
Initial	0.10	0.05	−0.15	0.01	−0.02	0.015
Desired	0.00	0.00	0.00	0.00	0.00	0.00

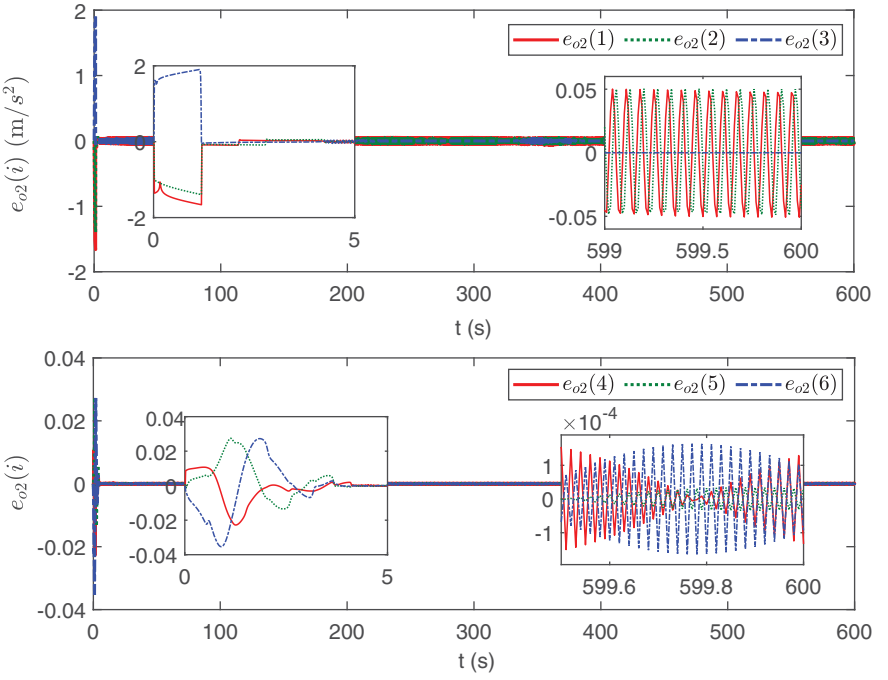

Figure 5. *The estimation error convergence curves of the proposed FT-DO.*

to effectively track the desired values. The initial tracking errors of orbit and attitude of the spacecraft are given in Table 1.

Remark 5: For the scenario of orbit control, adjusting the spacecraft's semi-major axis is sufficient. The reasons for choosing this scenario are as follows. The orbit control of a single satellite can be decoupled into in-plane and out-of-plane control. In-plane control is achieved by applying velocity impulses along the trajectory, resulting in changes in the satellite's semi-major axis a and eccentricity $\bar{e}$. On the other hand, out-of-plane control is achieved by applying normal velocity impulses perpendicular to the orbital plane, leading to changes in inclination i and right ascension of ascending node Ω. In general, in-plane and out-of-plane control are performed separately, as the latter often requires determining the timing of control initiation and the phase of control points within the orbital plane. However, since the timing of control initiation and the phase of control points are not the focus of this study, we simplify the analysis process by assuming a circular orbit for low Earth satellites and performing control within the orbital plane to investigate the effectiveness of the proposed controller. Then, the selection of the phase of control points can be ignored. The default initiation time in this paper is assumed to be the start of the simulation, i.e., $t = 0$. Therefore, this study only considers deviations in the semi-major axis, which can be seen as maneuvering the satellite from a circular orbit to another coplanar orbit.

https://doi.org/10.1017/aer.2024.2 Published online by Cambridge University Press

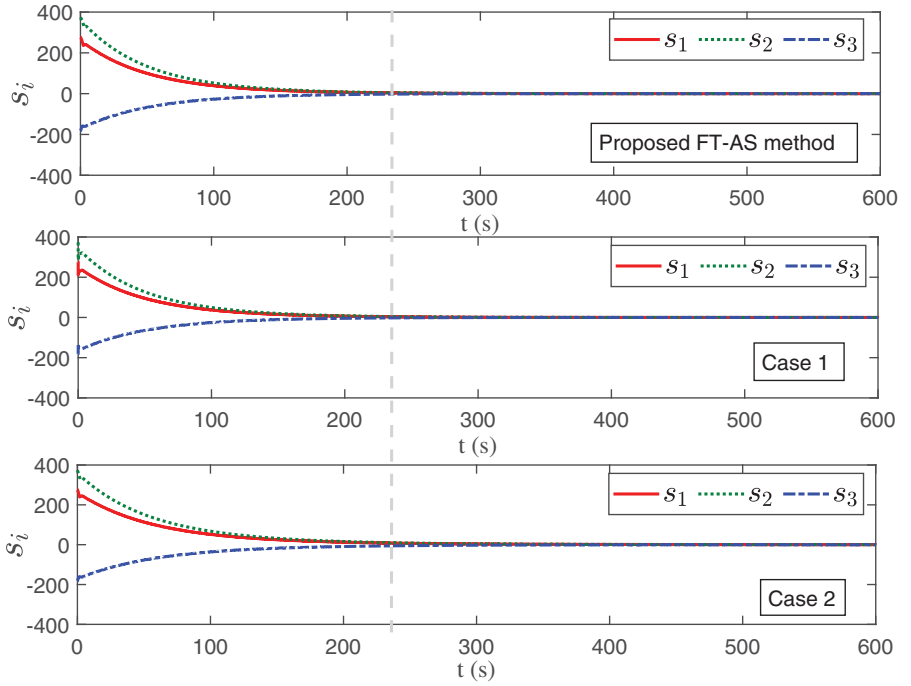

Figure 6. *Comparison of sliding mode surface convergence curves for position tracking error in three methods.*

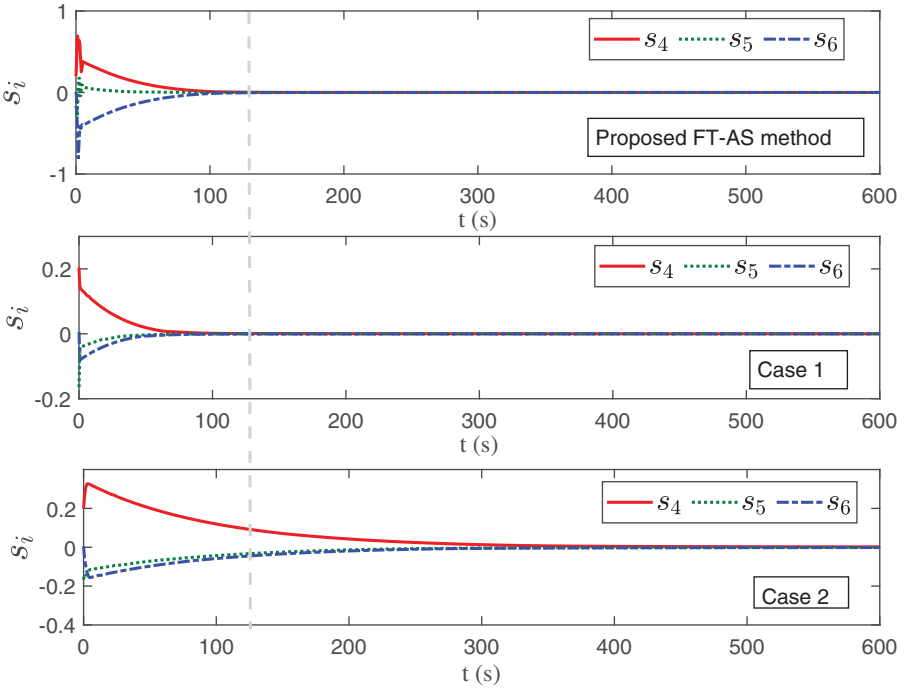

Figure 7. *Comparison of sliding mode surface convergence curves for velocity tracking error in three methods.*

https://doi.org/10.1017/aer.2024.2 Published online by Cambridge University Press

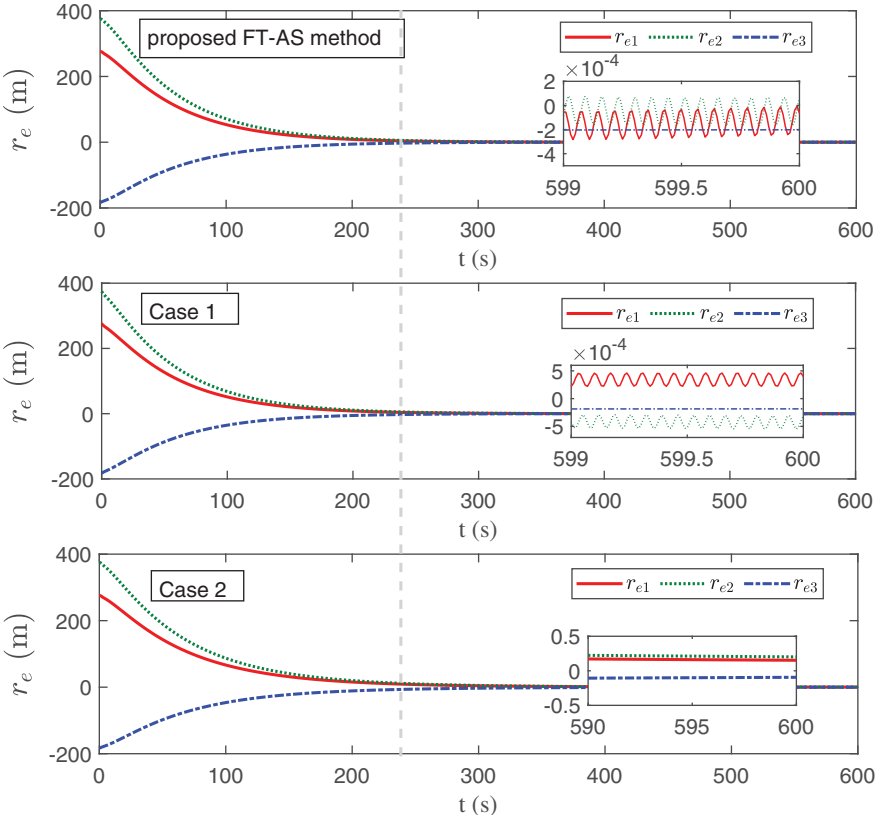

Figure 8. *Comparison of tracking errors convergence curves for position in three methods.*

The other parameters involved in the control process are as follows. The geocentric gravitational constant is $u_g = 3.986 \times 10^{14}$ $\mathrm{m^3 s^{-2}}$. The nominal mass and inertial matrix are $m_o = 600$ kg and $\boldsymbol{J_o} = \begin{bmatrix} 166.5 & 4.44 & 3.33 \\ 4.44 & 74 & 5.18 \\ 3.33 & 5.18 & 62.9 \end{bmatrix}$ $\mathrm{kgm^2}$ respectively. The external disturbance force and torque are $\boldsymbol{d_f} = [\sin(0.1t), \cos(0.2t), \sin(0.3t)]^T * 10^{-5}$ N and $\boldsymbol{d_\tau} = [2\sin(0.1t), 2\cos(0.2t), 2\sin(0.3t)]^T * 10^{-6}$ Nm. The uncertainties are: $\boldsymbol{\Delta J} = \begin{bmatrix} 0.1 + 0.01 * \sin(0.1t) & 0 & 0 \\ 0 & 0.1 + 0.01 * \sin(0.2t) & 0 \\ 0 & 0 & 0.1 + 0.01 * \sin(0.3t) \end{bmatrix}$ $\mathrm{kgm^2}$ and $\Delta m = 1 + 0.1 * \sin(0.1t)$ kg. The initial conditions of the fixed-time disturbance observer are $\boldsymbol{\vartheta_1}(0) = [0.00001, 0.00002, 0.00004, 0.00002, 0.00001, 0.00002]^T$ and $\boldsymbol{\vartheta_2}(0) = [1, 1, 1, 0.2, -0.4, 0.4]^T * 10^{-6}$. The focus of this paper revolves around the scenario of performing orbit and attitude adjustments within a small range on a small satellite. Therefore, the maximum control force and torque are preset as 2 N and 1 Nm, respectively.

The designed parameters of the observer are $p = 1.2$, $\lambda_1 = 0.5$, $\lambda_2 = 0.1$ and $\lambda_3 = 0.1$. The designed parameters of the controller (29) are $\nu_1 = 0.001$, $\eta_1 = 0.04$, $\nu_2 = 0.01$, $\eta_2 = 0.001$, $\frac{m_1}{n_1} = 2$, $\frac{p_1}{q_1} = 0.9$, $\frac{m_2}{n_2} = 1.1$, $\frac{p_2}{q_2} = 0.6$, $\varepsilon = 0.01$ and $\gamma = 0.05$.

https://doi.org/10.1017/aer.2024.2 Published online by Cambridge University Press

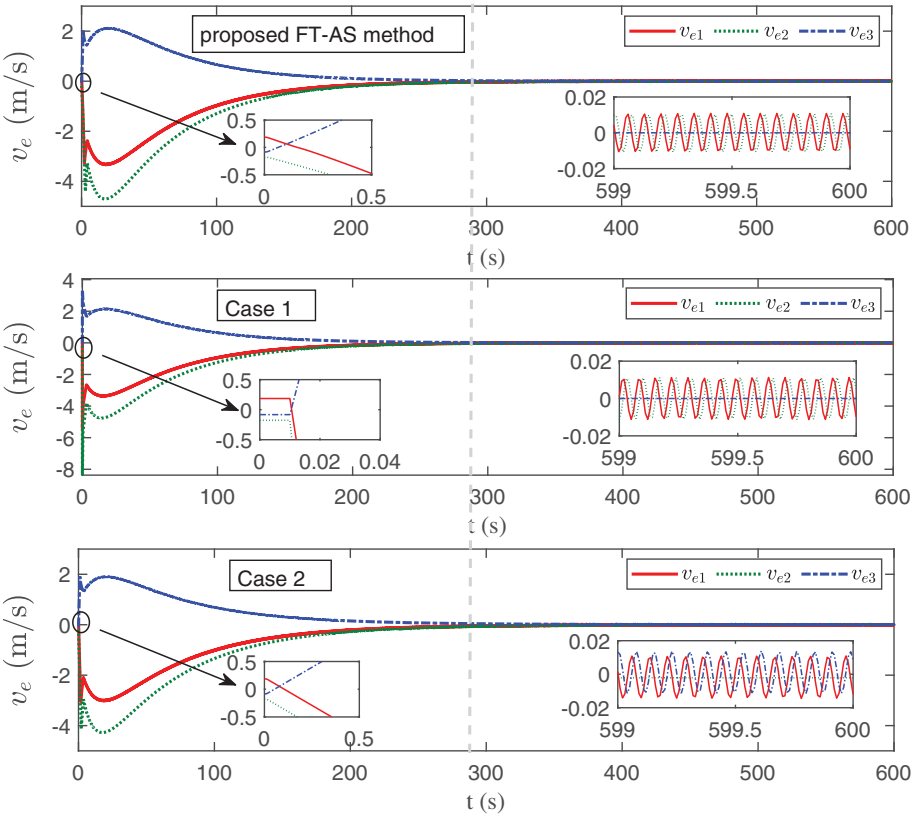

Figure 9. *Comparison of tracking errors convergence curves for velocity in three methods.*

5.2 Simulation implementation and results

5.2.1 Parameter adjustment criteria

Due to the multitude of parameters in both the controller and observer, their combined influence on the control system makes it challenging to establish a unified tuning criterion. In this paper, parameter tuning is conducted based on a trial-and-error approach, continually balancing convergence time and accuracy to obtain suitable parameters for the controller and observer. Nevertheless, this paper will analyse the impact of parameters on the system, providing readers with a set of criteria for independent selection.

Remark 6: The selection of parameters for the FT-DO adheres to the following basic criteria. The parameter p satisfies $p > 1$. The parameters $\lambda_1, \lambda_2, \lambda_3$ satisfy $\lambda_1 > \sqrt{2\lambda_3}$, $\lambda_2 > 0$, and $\lambda_3 > \delta d_s$, where δd_s is the bound of $||\dot{\boldsymbol{d}}_s||$. The effects of each parameter on the system are as follows. (1). λ_1 impact disturbance observation error, tracking error, control force, and torque. Increasing the value of λ_1 appropriately can reduce the convergence time of the disturbance observation error and improve the convergence accuracy. It also reduces the chattering of control force and torque. However, it leads to a decrease in the convergence accuracy of the tracking error. (2). λ_2 primarily affects the convergence time of the disturbance observer. A larger value of λ_2 results in a shorter convergence time. (3). λ_3 and p, while being adjusted within a small range while adhering to basic rules, have no significant impact on the system. However, it is important to note that these values should not be too large to prevent system instability. It is recommended to choose λ_3 within the range of $[0.05, 0.1]$ and p within the range of $[1,\ 2]$.

Remark 7: The selection of parameters for the FT-NTSM controller adheres to the following criteria. The parameters $\nu_1, \nu_2, \eta_1, \eta_2 > 0$. The parameters p_k, q_k, m_k and n_k, $(k = 1, 2)$ are positive odd integers

https://doi.org/10.1017/aer.2024.2 Published online by Cambridge University Press

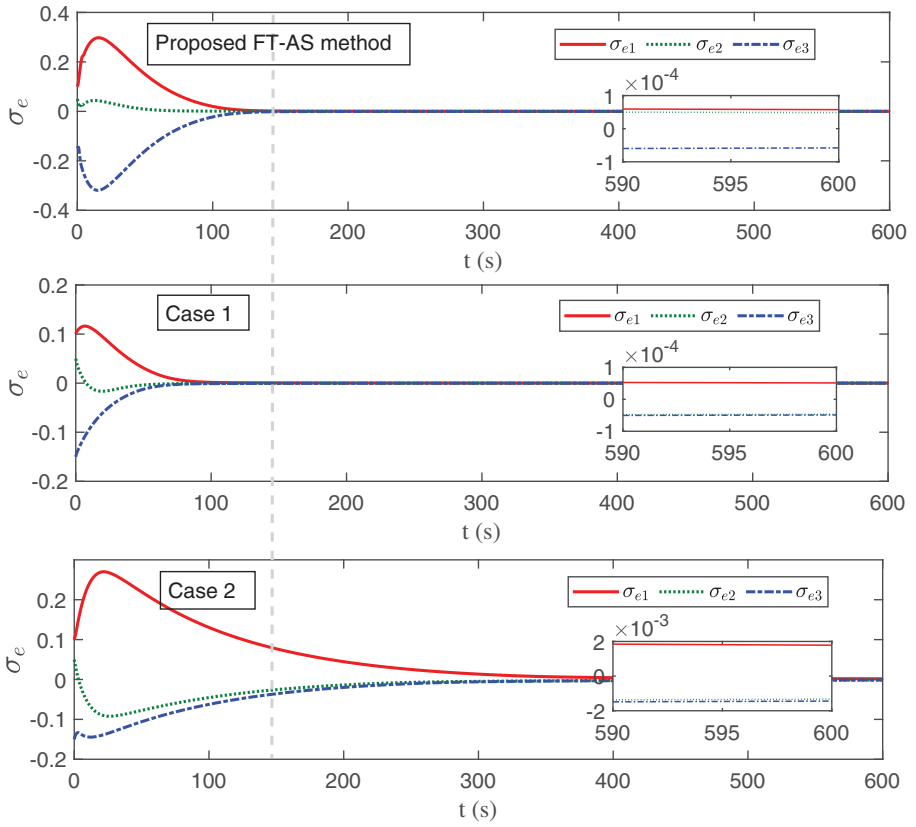

Figure 10. *Comparison of tracking errors convergence curves for MRPs in three methods.*

and satisfy $p_1 < q_1 < 2p_1, p_2 < q_2, m_k > n_k$ and $\frac{m_1}{n_1} - \frac{p_1}{q_1} > 1$. The effects of each parameter on the system are as follows. (1). Adjusting ν_1 within a reasonable range does not significantly affect the system's response. However, the value of ν_1 should not be too large to prevent system instability. (2). η_1 primarily affects the convergence time of the tracking error. Increasing η_1 within a reasonable range will result in a shorter convergence time of the tracking error and improve the system's dynamic response. (3). ν_2 primarily affects the convergence time of the tracking error and the sliding mode surface. Increasing ν_2 within a reasonable range leads to faster convergence. (4). η_2 primarily affects the convergence time and accuracy of the tracking error. Increasing η_2 within a reasonable range will result in a shorter convergence time and improved convergence accuracy of the tracking error. (5). Both m_1/n_1 and p_1/q_1 have similar effects on the system, and the larger the difference between them and 1, the shorter the convergence time of the tracking error. However, too large values for m_1/n_1 and too small values for p_1/q_1 can result in system instability. (6). The impact of m_2/n_2 on the system is not significant, but its value should not be too large as it can lead to system instability. p_2/q_2 has an impact on the dynamic response of the tracking error. If the value of p_2/q_2 is too small, it can lead to a poorer dynamic response of the tracking error. Additionally, too small and too large values of p_2/q_2 can result in longer convergence time and decreased convergence accuracy. (7). The impact of ε on the system is minimal and can be disregarded. Its value can be within the range of $[0.01,\ 0.001]$.

5.2.2 Simulation cases and results

The following two cases have been implemented to verify the effectiveness of the proposed FT-AS control method.

https://doi.org/10.1017/aer.2024.2 Published online by Cambridge University Press

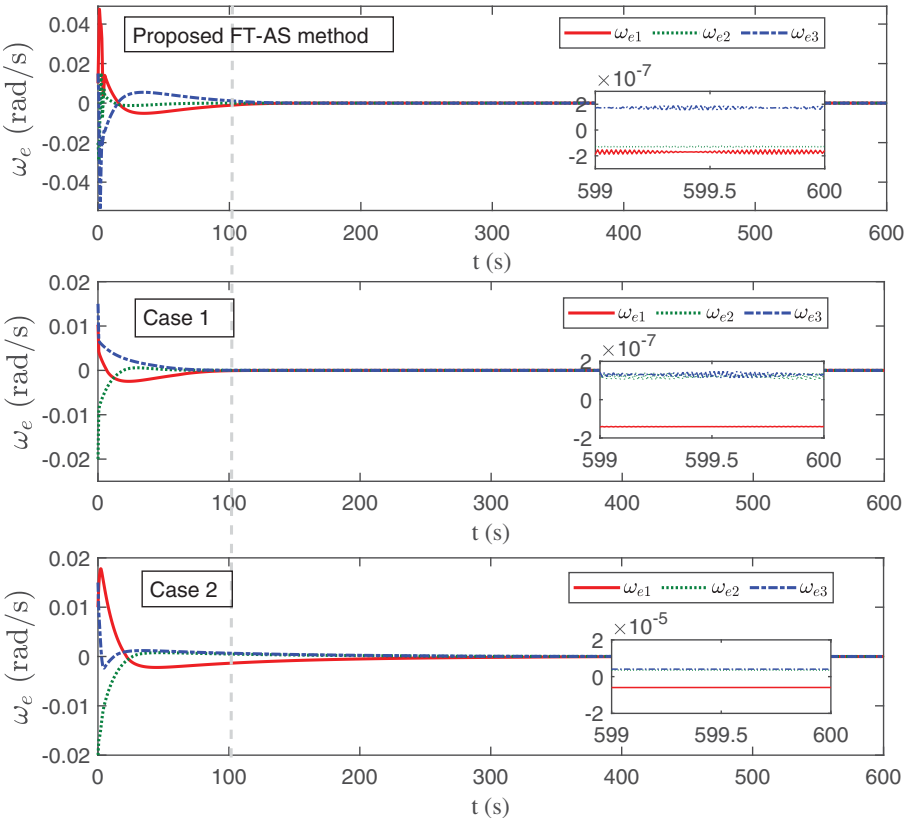

Figure 11. *Comparison of tracking errors convergence curves for angular velocity in three methods.*

Case 1: Compare the proposed FT-AS controller (29) with the traditional controller to verify its effectiveness in handling input saturation. The traditional controller is [24]

$$\boldsymbol{u_T} = (\boldsymbol{M_C}\boldsymbol{\kappa})^{-1}\left[\nu_1\left(\frac{m_1}{n_1}-\frac{p_1}{q_1}\right)\mathrm{diag}(\boldsymbol{e}_1)^{\frac{m_1}{n_1}-\frac{p_1}{q_1}-1}\boldsymbol{\kappa}^2\mathrm{diag}\,(\boldsymbol{e_2})\,\boldsymbol{e_2}-\frac{p_1}{q_1}\boldsymbol{\kappa}^{1-\frac{q_1}{p_1}}\boldsymbol{e_2}^{2-\frac{q_1}{p_1}}\right]$$
$$-\boldsymbol{M_C}^{-1}\left(\boldsymbol{h}+\hat{\boldsymbol{d}}+\gamma\,\mathrm{sign}\,(\boldsymbol{s})\right)-\boldsymbol{M_C}^{-1}\frac{p_1}{q_1}\boldsymbol{\kappa}^{-\frac{q_1}{p_1}}\boldsymbol{e_2}^{1-\frac{q_1}{p_1}}\mathrm{diag}\left(\boldsymbol{\phi}_\tau\right)\left(\nu_2\boldsymbol{s}^{\frac{m_2}{n_2}}+\eta_2\boldsymbol{s}^{\frac{p_2}{q_2}}\right) \tag{42}$$

where $\hat{\boldsymbol{d}}$ in (42) is the disturbance estimate that does not consider the adverse effects of input saturation.

Case 2: To demonstrate the effectiveness of the proposed FT-AS control system in reducing tracking error convergence time, it is compared with traditional sliding mode AS control systems with additional anti-saturation structure. The controller still uses (42).

The simulation results are shown in Figs. 5–13.

Figure 5 shows the estimation error convergence curve of the proposed FT-DO. The convergence time is within 5 s, which is very short. Thus, the influence of the convergence time of the proposed FT-DO on the overall system convergence time can be negligible. The estimation errors converge to 0.05 m/s^2 and $2 * 10^{-4}$, respectively, indicating that the proposed FT-DO can effectively estimate lumped disturbance. The observations of the disturbances will be fed back into the controller and suppressed using controller gains.

The comparisons between the proposed scheme and the above two cases are shown in Figs. 6–13.

https://doi.org/10.1017/aer.2024.2 Published online by Cambridge University Press

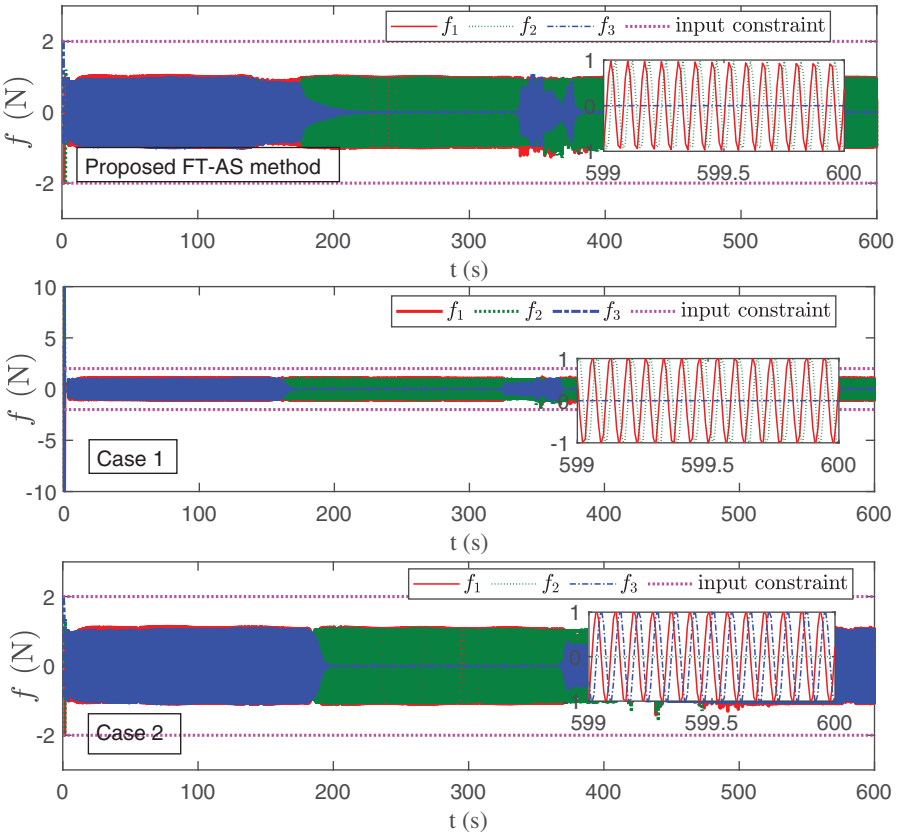

Figure 12. *Comparisons of input force.*

Figures 6 and 7 compare the convergence of the sliding surfaces for the three mentioned control methods. s_1, s_2 and s_3 represent the sliding surfaces for position tracking errors, while s_4, s_5 and s_6 represent the sliding surfaces for attitude tracking errors. As can be seen from Fig. 6, the proposed FT-AS method and the method used in Case 1 exhibit almost no difference in the convergence time of sliding surfaces s_1, s_2 and s_3. Therefore, the position tracking errors of these two methods reach the sliding surfaces almost simultaneously. However, in Case 2, which involves an additional saturation structure, the time it takes for the position tracking errors to reach the sliding surfaces is the longest, indicating that its performance is significantly inferior to the previous two methods. The sliding surfaces s_4, s_5, and s_6 are shown in Fig. 7. The method in Case 1 exhibits the shortest convergence time, followed by the proposed FT-AS method. The worst performance is still Case 2. This indicates that the additional anti-saturation structure significantly affects the convergence time of the sliding surface. Therefore, it is meaningful to design a more concise control loop without the additional anti-saturation subsystem.

Figures 8 and 9 demonstrate the convergence of position and velocity tracking errors for the three methods. For the position tracking errors $\boldsymbol{r_e}$ shown in Fig. 8, Case 2 exhibits the poorest convergence time and accuracy. The method in Case 1 and the proposed FT-AS method have similar convergence times for position tracking errors, but the FT-AS method outperforms in terms of convergence accuracy. The convergence accuracy by the proposed FT-AS method is within $2 * 10^{-4}$ m, Case 1 is within $5 * 10^{-4}$ m, and Case 2 is within 0.5 m. For velocity tracking errors $\boldsymbol{v_e}$ shown in Fig. 9, although the three methods have similar convergence accuracy, both Case 1 and the proposed FT-AS method outperform Case 3 in terms of convergence time. Therefore, the proposed FT-AS method exhibits advantages in convergence time and accuracy of position and velocity tracking errors.

https://doi.org/10.1017/aer.2024.2 Published online by Cambridge University Press

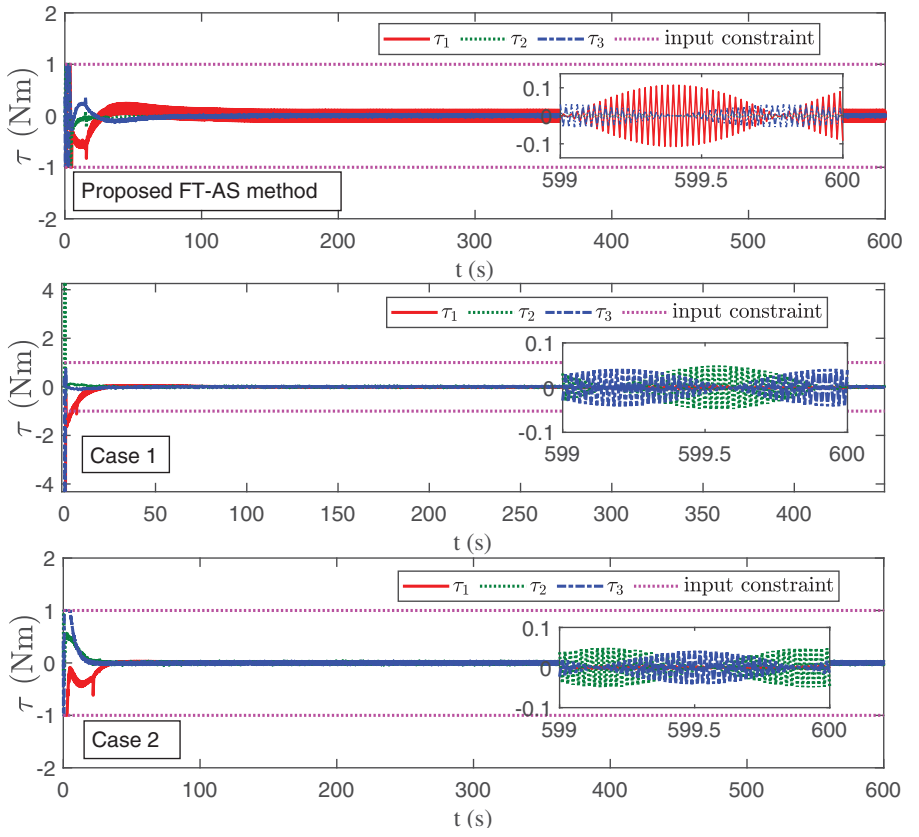

Figure 13. *Comparisons of input torque.*

The attitude tracking errors of the three methods are shown in Figs. 10 and 11. For the tracking errors of the MRPs and the angular velocity, the shortest convergence time is Case 1, followed by the proposed FT-AS method, both of which have a shorter convergence time than Case 2. In addition, for the convergence accuracy of attitude tracking errors, the MRPs and angular velocity of the proposed method and Case 1 converge to $1 * 10^{-4}$ and $2 * 10^{-7}$ rad/s, respectively. However, the MRPs and angular velocity of Case 2 converge to $2 * 10^{-3}$ and $2 * 10^{-5}$ rad/s, respectively. Therefore, the proposed FT-AS method and the method used in Case 1 perform well.

Figures 12 and 13 illustrate the control force and control moment curves. Both the proposed FT-AS method and Case 2 method ensure that the control force and control moment remain within the specified limits. In Case 1, however, without saturation limits, the control force and moment initially exceed the actuator's limits. Such large control energy will accelerate the convergence of the sliding mode surface, position tracking error, and attitude tracking error. Nonetheless, this poses a danger in practical applications as it may cause damage to the spacecraft's actuators. At the beginning of the simulation, all three methods exhibit high control force and moment, as large forces and moments are required for orbital and attitude manoeuvres. In the later stages, the control force and torque stabilise within the desired range, which is utilised to overcome spatial disturbances.

Nevertheless, it should be noted that the proposed FT-AS method still has some drawbacks, such as incomplete elimination of control force and moment chattering. Furthermore, the estimation of the system's convergence time is relatively conservative.

In conclusion, the FT-DO proposed in this paper can effectively suppress the adverse effects of input saturation. The proposed FT-AS control system has higher control accuracy and shorter convergence

https://doi.org/10.1017/aer.2024.2 Published online by Cambridge University Press

time. Compared to traditional control schemes with additional saturation structures, this scheme simplifies the entire control system structure and has good control performance.

6.0 Conclusion

A FT-AS scheme with a simple control structure is proposed for the spacecraft's 6-DOF tracking motion. The proposed approach achieves fixed-time stability for spacecraft with input saturation and offers a more concise control loop than traditional anti-saturation methods. This paper directly feeds the input overshoot into the tracking error dynamical system, converting its impact into a modified disturbance term. This term is then observed using the designed FT-DO. This approach avoids adding additional structures in the control loop, resulting in a simpler and more modular system. The FT-DO in this paper has fewer parameters, which is easy to adjust. Based on the FT-DO, a FT-NTSM controller is designed to ensure the system's fixed-time stability. The simulation results demonstrate that the designed FT-DO can accurately observe the disturbances that include the effects of input overshoot. The proposed controller guarantees that the control input remains within the prescribed limits. Compared to the traditional methods of adding anti-saturation subsystems, the proposed method exhibits faster convergence speed and achieves comparable or even higher tracking accuracy for both position and attitude. In the future, it is imperative to research mitigating chattering in sliding mode control systems to enhance their engineering applicability. Additionally, considering the detrimental effects of actuator failures on the stability of spacecraft flight, fixed-time fault-tolerant control is also worth further research.

Acknowledgements. This work is supported by Shanghai Excellent Academic Leader (No.21XD1401700) and the National Key Research and Development Program (2021YFC3000405).

Competing interests. The authors declare that they have no known competing financial interests or personal relationships that could have appeared to influence the work reported in this paper.

References

[1] Amrr, S.M. and Nabi, M. Finite-time fault tolerant attitude tracking control of spacecraft using robust nonlinear disturbance observer with anti-unwinding approach, *Adv. Space. Res.*, 2020, **66**, (7), pp 1659–1671.
[2] Bunryo, Y., Satoh, S., Shoji, Y. and Yamada, K. Feedback attitude control of spacecraft using two single gimbal control moment gyros, *Adv. Space. Res.*, 2021, **68**, (7), pp 2713–2726.
[3] Dony, M.N. and Dong, W. Distributed robust formation flying and attitude synchronization of spacecraft, *J. Aerospace. Eng.*, 2021, **34**, (4), pp 4021015.1–4021015.11.
[4] Li, C., Zou, H., Shi, D., Song, J. and Wang, J. Proportional-integral-type event-triggered coupled attitude and orbit tracking control using dual quaternions, *IEEE Trans. Aero. Elec. Sys.*, 2022, **58**, (4), pp 3021–3036.
[5] Dong, H and Yang, X. Finite-time prescribed performance control for space circumnavigation mission with input constraints and measurement uncertainties, *IEEE Trans. Aero. Elec. Sys.*, 2022, **58**, (4), pp 3209–3222.
[6] Wang, L., Liu, J., Zhou, Z. and Li, Y. A two-stage dimension-reduced dynamic reliability evaluation (TD-DRE) method for vibration control structures based on interval collocation and narrow bounds theories, *ISA Trans.*, 2023, **136**, pp 622–639.
[7] Wang, L., Zhao, Y., Liu, J. and Zhou, Z. Uncertainty-oriented optimal PID control design framework for piezoelectric structures based on subinterval dimension-wise method (SDWM) and non-probabilistic time-dependent reliability (NTDR) analysis, *J. Sound. Vib.*, 2023, **549**, (2023), pp 117588.
[8] Wang, L.,Zhou, Z. and Liu, J. Double-time-scale non-probabilistic reliability-based controller optimization for manipulator considering motion error and wear growth, ISA Trans., 2023, in press.
[9] Utkin, V.I. and Poznyak, A.S. Adaptive sliding mode control with application to super-twist algorithm: equivalent control method, *Automatica*, 2013, **49**, (2013), pp 39–47.
[10] Jiang, S., Liu,C. and Gao,Y. MIMO adaptive high-order sliding mode control for quadrotor attitude tracking, *J. Aerospace. Eng.*, 2021, **34**, (4), pp 4021022.1–4021022.10.
[11] Dey, S., Giri, K.D., Gaurav, K. and Laxmi, V. Robust nonsingular terminal sliding mode attitude control of satellites, *J. Aerospace. Eng.*, 2021, **34**, (1), pp 6020003.1–6020003.9.
[12] Dehkordi, D.M. and Danesh, M. Positionable rotor quadrotor: dynamic modeling and adaptive finite-time sliding-mode controller design, *J. Guid. Control. Dynam.*, 2022, **45**, (3), pp 424–433.
[13] Alipour,M.R., Saberi, F.F. and Kabganian, M. Modelling, design and experimental implementation of non-linear attitude tracking with disturbance compensation using adaptive-sliding control based on quaternion algebra, *Aeronaut. J.*, 2018, **122**, (1247), pp 148–171.

https://doi.org/10.1017/aer.2024.2 Published online by Cambridge University Press

[14] Pukdeboon, C. and Kumam, P. Robust optimal sliding mode control for spacecraft position and attitude maneuvers, *Aerosp. Sci. Technol.*, 2015, **43**, pp 329–342.
[15] Lee, D. and Vukovich, G. Adaptive sliding mode control for spacecraft body-fixed hovering in the proximity of an asteroid, *Aerosp. Sci. Technol.*, 2015, **46**, pp 471–483.
[16] Li, F., Hu, M. and Yang, M. Rotational and relative translational control for satellite electromagnetic formation flying in low earth orbit, *Aircr. Eng. Aerosp. Tec.*, 2017, **89**, (6), pp 815–825.
[17] Wang, J. and Sun, Z. 6-DOF robust adaptive terminal sliding mode control for spacecraft formation flying, *Acta Astronaut.*, 2012, **73**, pp 76–87.
[18] Polyakov, A. Nonlinear feedback design for fixed-time stabilization of linear control systems, *IEEE Trans. Automat. Contr.*, 2012, **57**, (8), pp 2106–2110.
[19] Zuo, Z. Non-singular fixed-time terminal sliding mode control of non-linear systems, *IET Control Theory A.*, 2015, **9**, (4), pp 545–552.
[20] Yun, Y.,Tang, S., and Guo, J. Smooth adaptive fixed time convergent controller design for BTT missiles with uncertainties, *Aeronaut. J.*, 2020, **124**, (1273), pp 323–345.
[21] Jiang, B., Hu, Q. and Friswell, M.I. Fixed-time attitude control for rigid spacecraft with actuator saturation and faults, *IEEE Trans. Contr. Syst. T.*, 2016, **24**, (5), pp 1892–1898.
[22] Chen, Q., Xie, S.Z., Sun, M.X. and He, X. Adaptive nonsingular fixed-time attitude stabilization of uncertain spacecraft, *IEEE Trans. Aero. Elec. Sys.*, 2018, **54**, (6), pp 2937–2950.
[23] Han, Z., Wang, M., Yan, X. and Qian, H. Adaptive fixed-time nonsingular terminal sliding mode attitude tracking control for spacecraft with actuator saturations and faults, *Int. J. Aerospace Eng.*, 2021, **2021**, pp 8838784.
[24] Wu, S., Chen, L., Zhang, D., Chen, J. and Shao, X. Disturbance observer based fixed time sliding mode control for spacecraft proximity operations with coupled dynamics, *Adv. Space. Res.*, 2020, **66**, (9), pp 2179–2193.
[25] Errouissi, R. and Al-Durra, A. Disturbance-observer-based control for dual-stage grid-tied photovoltaic system under unbalanced grid voltages, *IEEE Trans. Ind. Electron.*, 2019, **66**, (11), pp 8925–8936.
[26] Sun, L. Adaptive fuzzy relative pose control of spacecraft during rendezvous and proximity maneuvers, *IEEE Trans. Fuzzy Syst.*, 2018, **26**, (6), pp 3440–3451.
[27] Zhu, X., Chen, J. and Zhu, Z.H. Adaptive sliding mode disturbance observer-based control for rendezvous with non-cooperative spacecraft, *Acta Astronaut.*, 2021, **183**, pp 59–74.
[28] Sun, L. and Zheng, Z.W. Disturbance observer-based robust saturated control for spacecraft proximity maneuvers, *IEEE Trans. Contr. Syst. T.*, 2018, **26**, (2), pp 684–692.
[29] Hu, Q., Jiang, B. and Friswell M.I. Robust saturated finite time output feedback attitude stabilization for rigid spacecraft, *J. Guid. Control. Dynam.*, 2014, **37**, (6), pp 1914–1929.
[30] Sun, L. and Jiang, J. Adaptive control of space proximity missions with constrained relative states, faults and saturation, *Acta Astronaut.*, 2020, **174**, pp 211–218.
[31] Sun, L. and Zheng, Z. Disturbance-observer-based robust backstepping attitude stabilization of spacecraft under input saturation and measurement uncertainty, *IEEE Trans. Ind. Electron.*, 2017, **64**, (10), pp 7994–8002.
[32] Hu, Q., Li, B. and Qi, J. Disturbance observer based finite-time attitude control for rigid spacecraft under input saturation, *Aerosp. Sci. Technol.*, 2014, **39**, pp 13–21.
[33] Zhuang, M., Tan, L., Li, K. and Song, S. Fixed-time formation control for spacecraft with prescribed performance guarantee under input saturation, *Aerosp. Sci. Technol*, 2021, **119**, pp 107176.
[34] Basin, M., Panathula, C.B. and Shtessel, Y. Multivariable continuous fixed-time second-order sliding mode control: design and convergence time estimation, *IET Control Theory A.*, 2017, **11**, (8), pp 1104–1111.
[35] Kristiansen, R., Groli, E.I., Nicklasson, P.J. and Gravdahl, J.T. A model of relative translation and rotation in leader-follower spacecraft formations, Model. Identif. Control, 2007, **28**, (1), pp 3–14.
[36] Zhang, C., Ma, G., Sun, Y. and Li, C. Prescribed performance adaptive attitude tracking control for flexible spacecraft with active vibration suppression, *Nonlinear Dyn.*, 2019, **2019**, (96), pp 1909–1926.
[37] Sun, L., Huo, W. and Jiao, Z. Adaptive backstepping control of spacecraft rendezvous and proximity operations with input saturation and full-state constraint, *IEEE T. Ind. Electron.*, 2017, **64**, (1), pp 480–492.
[38] Zhang, C., Wang, J., Zhang, D. and Shao, X. Learning observer based and event-triggered control to spacecraft against actuator faults, *Aerosp. Sci. Technol*, 2018, **78**, pp 522–530.
[39] Wen, C., Zhou, J., Liu, Z. and Su, H. Robust adaptive control of uncertain nonlinear systems in the presence of input saturation and external disturbance, *IEEE T. Automat. Contr.*, 2011, **56**, (7), pp 1672–1678.

APPENDIX

A Relationship between MRPs and angular velocity

The attitude kinematic differential equation of the MRPs in matrix form is:

$$\dot{\boldsymbol{\sigma}} = \frac{1}{4}\begin{bmatrix} 1-\boldsymbol{\sigma}^T\boldsymbol{\sigma}+2\sigma_1^2 & 2(\sigma_1\sigma_2-\sigma_3) & 2(\sigma_1\sigma_3+\sigma_2) \\ 2(\sigma_2\sigma_1+\sigma_3) & 1-\boldsymbol{\sigma}^T\boldsymbol{\sigma}+2\sigma_2^2 & 2(\sigma_2\sigma_3-\sigma_1) \\ 2(\sigma_3\sigma_1-\sigma_2) & 2(\sigma_3\sigma_2+\sigma_1) & 1-\boldsymbol{\sigma}^T\boldsymbol{\sigma}+2\sigma_3^2 \end{bmatrix}\begin{bmatrix} w_1 \\ w_2 \\ w_3 \end{bmatrix}] \tag{A1}$$

https://doi.org/10.1017/aer.2024.2 Published online by Cambridge University Press

The corresponding vector form of the above equation is:

$$\dot{\boldsymbol{\sigma}} = \frac{1}{4}\left[\left(1-\boldsymbol{\sigma}^T\boldsymbol{\sigma}\right)\boldsymbol{I}_3 + 2\psi\left(\boldsymbol{\sigma}\right) + 2\boldsymbol{\sigma}\boldsymbol{\sigma}^T\right]\boldsymbol{w} = \frac{1}{4}\left[\boldsymbol{B}(\boldsymbol{\sigma})\right]\boldsymbol{w} \tag{A2}$$

The matrix $[\boldsymbol{B}(\boldsymbol{\sigma})]$ transforms the angular velocity $\boldsymbol{w}$ into $\dot{\boldsymbol{\sigma}}$. The matrix $[\boldsymbol{B}(\boldsymbol{\sigma})]$ is almost orthogonal except for a generally non-unit scaling factor. The inverse of $[\boldsymbol{B}(\sigma)]$ is:

$$[\boldsymbol{B}(\boldsymbol{\sigma})]^{-1} = \frac{1}{(1+\sigma^T\sigma)^2}[\boldsymbol{B}(\boldsymbol{\sigma})]^T \tag{A3}$$

The proof of Equation (A3) is as follows. Based on (A2), $[\boldsymbol{B}(\boldsymbol{\sigma})\,]^T\,[\boldsymbol{B}(\boldsymbol{\sigma})]$ can be written as:

$$\left[\boldsymbol{B}(\boldsymbol{\sigma})\right]^T[\boldsymbol{B}(\boldsymbol{\sigma})] = \left[\left(1-\boldsymbol{\sigma}^T\boldsymbol{\sigma}\right)\boldsymbol{I}_3 - 2\psi(\boldsymbol{\sigma}) + 2\boldsymbol{\sigma}\boldsymbol{\sigma}^T\right]\left[\left(1-\boldsymbol{\sigma}^T\boldsymbol{\sigma}\right)\boldsymbol{I}_3 + 2\psi(\boldsymbol{\sigma}) + 2\boldsymbol{\sigma}\boldsymbol{\sigma}^T\right] \tag{A4}$$

After carrying out the matrix multiplications, $[\boldsymbol{B}(\boldsymbol{\sigma})\,]^T\,[\boldsymbol{B}(\boldsymbol{\sigma})]$ can be reduced to

$$[\boldsymbol{B}(\boldsymbol{\sigma})]^T[\boldsymbol{B}(\boldsymbol{\sigma})] = (1-\boldsymbol{\sigma}^T\boldsymbol{\sigma})^2\boldsymbol{I}_3 - 4\psi^2(\boldsymbol{\sigma}) + 4\boldsymbol{\sigma}\boldsymbol{\sigma}^T \tag{A5}$$

$[\boldsymbol{B}(\boldsymbol{\sigma})]^T\,[\boldsymbol{B}(\boldsymbol{\sigma})]$ can be further simplified using the identity $\psi^2(\boldsymbol{\sigma}) = \boldsymbol{\sigma}\boldsymbol{\sigma}^T - \boldsymbol{\sigma}^T\boldsymbol{\sigma}\boldsymbol{I}_3$ to

$$[\boldsymbol{B}(\boldsymbol{\sigma})]^T[\boldsymbol{B}(\boldsymbol{\sigma})] = (1+\boldsymbol{\sigma}^T\boldsymbol{\sigma})^2\boldsymbol{I}_3 \tag{A6}$$

Therefore, the Equation (A3) holds. The inverse transformation of Equations (A1) and (A2) in matrix and vector forms can be written as (A7) and (A8), respectively.

$$\boldsymbol{w} = \frac{4}{(1+\sigma^T\sigma)^2}[\boldsymbol{B}(\boldsymbol{\sigma})]^T\dot{\boldsymbol{\sigma}} \tag{A7}$$

$$\boldsymbol{w} = \frac{4}{(1+\boldsymbol{\sigma}^T\boldsymbol{\sigma})^2}\left[\left(1-\boldsymbol{\sigma}^T\boldsymbol{\sigma}\right)\boldsymbol{I}_3 - 2\psi(\boldsymbol{\sigma}) + 2\boldsymbol{\sigma}\boldsymbol{\sigma}^T\right]\dot{\boldsymbol{\sigma}} \tag{A8}$$

In this paper, define $G(\boldsymbol{\sigma}) = \frac{1}{4}\left[\boldsymbol{B}(\boldsymbol{\sigma})\right]$ and $G(\boldsymbol{\sigma})^{-1} = \frac{4}{(1+\boldsymbol{\sigma}^T\boldsymbol{\sigma})^2}\left[\left(1-\boldsymbol{\sigma}^T\boldsymbol{\sigma}\right)\boldsymbol{I}_3 - 2\psi(\boldsymbol{\sigma}) + 2\boldsymbol{\sigma}\boldsymbol{\sigma}^T\right]$. The first derivatives of $G(\boldsymbol{\sigma})$ and $G(\boldsymbol{\sigma})^{-1}$ are respectively given by:

$$\begin{aligned}\dot{G}(\boldsymbol{\sigma}) &= \frac{1}{4}\left[-2\boldsymbol{\sigma}^T\dot{\boldsymbol{\sigma}}\boldsymbol{I}_3 + 2\psi(\dot{\boldsymbol{\sigma}}) + 2\dot{\boldsymbol{\sigma}}\boldsymbol{\sigma}^T + 2\boldsymbol{\sigma}\dot{\boldsymbol{\sigma}}^T\right] \\ &= \frac{1}{2}\left[-\boldsymbol{\sigma}^T\dot{\boldsymbol{\sigma}}I_3 + \psi(\dot{\boldsymbol{\sigma}}) + \dot{\boldsymbol{\sigma}}\boldsymbol{\sigma}^T + \boldsymbol{\sigma}\dot{\boldsymbol{\sigma}}^T\right]\end{aligned} \tag{A9}$$

$$\begin{aligned}\dot{G}(\boldsymbol{\sigma})^{-1} &= \frac{-16\boldsymbol{\sigma}^T\dot{\boldsymbol{\sigma}}}{(1+\boldsymbol{\sigma}^T\boldsymbol{\sigma})^4}\left[\left(1-\boldsymbol{\sigma}^T\boldsymbol{\sigma}\right)I_3 - 2\psi(\boldsymbol{\sigma}) + 2\boldsymbol{\sigma}\boldsymbol{\sigma}^T\right] \\ &\quad + \frac{4}{(1+\boldsymbol{\sigma}^T\boldsymbol{\sigma})^2}\left[-2\boldsymbol{\sigma}^T\dot{\boldsymbol{\sigma}}I_3 - 2\psi(\dot{\boldsymbol{\sigma}}) + 2\dot{\boldsymbol{\sigma}}\boldsymbol{\sigma}^T + 2\boldsymbol{\sigma}\dot{\boldsymbol{\sigma}}^T\right] \\ &= \frac{8}{(1+\boldsymbol{\sigma}^T\boldsymbol{\sigma})^2}\left[-\boldsymbol{\sigma}^T\dot{\boldsymbol{\sigma}}I_3 - \psi(\dot{\boldsymbol{\sigma}}) + \dot{\boldsymbol{\sigma}}\boldsymbol{\sigma}^T + \boldsymbol{\sigma}\dot{\boldsymbol{\sigma}}^T\right] \\ &\quad - \frac{16\boldsymbol{\sigma}^T\dot{\boldsymbol{\sigma}}}{(1+\boldsymbol{\sigma}^T\boldsymbol{\sigma})^4}\left[\left(1-\boldsymbol{\sigma}^T\boldsymbol{\sigma}\right)\boldsymbol{I}_3 - 2\psi(\boldsymbol{\sigma}) + 2\boldsymbol{\sigma}\boldsymbol{\sigma}^T\right]\end{aligned} \tag{A10}$$

Cite this article: Wei X., Tian Y., Wu S., Zhang D., Shao X. and Chen L. (2024). Fixed-time anti-saturation control with concise system structure for the 6-DOF motion of spacecraft. *The Aeronautical Journal*, **128**, 1627–1651. https://doi.org/10.1017/aer.2024.2